High lubricity meets load capacity: Cartilage mimicking bilayer structure by brushing up stiff hydrogels from sub-surface

Mingming Rong[#], Hui Liu[#], Michele Scaraggi, Yanyan Bai, Luyao Bao, Shuanhong Ma, Zhengfeng Ma, Meirong Cai[1], Daniele Dini*, Feng Zhou**

Dr. M. Rong, Dr. H. Liu, Dr. Y. Bai, Dr. L. Bao, Dr. Z. Ma, Prof. S. Ma, Prof. M. Cai, Prof. F. Zhou
State Key Laboratory of Solid Lubrication, Lanzhou Institute of Chemical Physics, Chinese Academy of Sciences, Lanzhou, 730000, China
E-mail: zhouf@licp.cas.cn; mashuanhong@licp.cas.cn

Dr. M. Rong, Dr. H. Liu, Dr. Y. Bai,
China University of the Chinese Academy of Sciences, Beijing, 100049, China

Prof. M. Scaraggi,
Universitá del Salento, 73100 Monteroni-Lecce, Italy, EU
Imperial College London, London SW7 2AZ, UK
Istituto Italiano di Tecnologia (IIT), Center for Bio-Molecular Nanotechnologies, 73010 Arnesano (Lecce), Italy, EU

Prof. D. Dini
Imperial College of London, London SW7 2AZ, UK
E-mail: d.dini@imperial.ac.uk

Note: *[#]M. Rong. and H.Liu. contributed equally to this work.*

Author Contributions

The work is the result of a strong and long-term collaboration (~2 years) established with Professor Zhou's group at the State Key Laboratory of Solid Lubrication, Chinese Academy of Sciences, and Professor Scaraggi at the University of Salento, and Professor Dini at Imperial College of London.

F.Z. and S.M. conceived the idea and designed the experiment; M.M.R. and H.L. carried out the experiments; M.M. R analyzed the data and wrote the first manuscript draft; M.S., D.D., Y.B. and L.B. carried out the theoretical studies and the simulations. F.Z., D.D., M.S. and S.M revised the draft and finalized the paper. All the authors contributed to scientific discussion of the article and its writing.

Keywords: hydrogels; polymer brushes; sub-surface polymerization; low friction; high load-bearing.

Abstract

Natural articular cartilage has ultralow friction even at high squeezing pressure. Biomimicking cartilage with soft materials has been and remains a grand challenge in the fields of materials science and engineering. Inspired by the unique structural features of the articular cartilage, as well as by its remarkable lubrication mechanisms dictated by the properties of the superficial layers, herein a novel architype of cartilage-mimicking bilayer material by robustly entangling thick hydrophilic polyelectrolyte brushes into the sub-surface of a stiff hydrogel substrate is developed. The topmost soft polymer layer provides effective aqueous lubrication, whereas the stiffer hydrogel layer used as a substrate delivers the load-bearing capacity. Their synergy is capable of attaining low friction coefficients (order 0.010) under heavily loaded conditions (order 10 MPa contact pressure) in water environment, a performance incredibly close to that of natural articular cartilage. The bioinspired material can maintain low friction even when subjected to 50k reciprocating cycles under high contact pressure, with almost no wear observed on the sliding track. These findings are theoretically explained and compounded by multi-scale simulations used to shed light on the mechanisms responsible for this remarkable performance. This work opens innovative technology routes for developing cartilage-mimicking ultralow friction soft materials.

1. Introduction

The human articular cartilage, a typical nature-optimized soft matter, is mainly composed of a large amount of collagen fibers and proteoglycans, which cooperate with synovial fluid in the joint cavity to realize both high load-bearing (3~18 MPa) and extremely low friction (0.001~0.030) in a wide range of sliding velocities and contact dynamics.[1] Inspired by this fascinating phenomenon, scientists have used hydrogels as a route to mimic, at least partially, some of the features characterizing such natural aqueous lubricating system. Hydrogels are usually hydrophilic polymer networks which exhibit soft elasticity and hydration features,[2] as well as typically low friction (compared to the common picture of dissipation in solid polymers), along with customizable biocompatibility,[3] making them potential candidates e.g. for replacing articular cartilage.[4] Many efforts have been devoted to develop hydrogel materials with outstanding lubrication performance.[5] However, an extremely low friction (low wall shear stress) requires hydrogel to have a large degree of hydration, which in turn negatively impacts the load-bearing capacity due to severe deformation experienced by the gel under contact dynamics.[6] Several strategies have been conceived to engineer high strength hydrogels.[7] For example, some of us reported on a novel dual cross-linked hydrogels with excellent compressive elastic modulus (larger than 30 MPa) and tensile strength (larger than 6 MPa).[8] Furthermore, by optimizing the experimental parameters upon employing a pre-stretching strategy, the tensile strength could reach values as high as ≈40 MPa.[9] Nevertheless, increasing the mechanical strength of hydrogels improves the load-bearing capacity, but at the cost of deep lowering the surface hydration degree, which in turn negatively affects the fiction coefficient. Therefore, simultaneously achieving both high load-bearing, long wear resistance and low friction properties, under in-vitro physiological conditions for e.g. cartilage replacement applications, is the current scientific challenge in the design of biomimicking synthetic articular cartilage.

In order to address the challenge, we looked back the mechanisms of natural system. The articular cartilage is constituted of the outer, middle, deep and calcified zone (basically a cellular arrangement within fibrillar collagen with different distribution/density and extracellular matrix).[10] The tribological side of the cartilage, i.e. the outer zone in contact with synovial fluid, has high water content (highly hydrated soft layer) in order to minimize the joint sliding friction also thanks to the weeping lubrication; the other side, i.e. the thicker middle and deep zone, has higher density of collagen fibrils to provide subsurface contact stress attenuation, where the subsurface stresses originate from the articulation contact stresses.[11] As a result, the synergy of the composite biphasic structure endows the articular cartilage with both extremely low friction and excellent antiwear property. Furthermore, by anchoring the collagen fibrils of the deep zone perpendicularly to the articular cartilage surface, the calcified zone is kinematically constrained onto the cartilage, leading to an effective continuous stress attenuation across the composite tissue.

Inspired by this, we propose a novel, robust, tough biomimicking hydrogel material obtained by grafting hydrophilic polyelectrolyte brushes onto a sub-surface of a stiff hydrogel to form a bilayer structure. The top layer consists of hydrophilic polymer brushes whose beds are covalently entangled below the surface (several tens of micrometers) of the stiff hydrogel, leading to a continuous transition from the top hydrated layer to the underlying bulk hydrogel, exhibiting no delamination. This results in a man-made (simplified) realistic prototype of cartilage-like material. The top composite layer shows excellent lubricity, whereas the bottom hydrogel contributes to the broadening (thus reducing) of the subsurface contact stress across the slab. A multiscale contact model for the dual layer hydrogel was developed to interpret the friction mechanisms, and to provide the theoretical tools for the design of water-based ultralow friction materials for human and mechatronics applications.

2. Results and Discussions

2.1. Preparation and components analysis of the bi-layered composite hydrogel

The preparation of the high strength hydrogel grafted with polymer brushes (HHy-g-PBs) is depicted in **Figure 1**, and briefly summarized in the following. A HHy-g-PBs is realized performing subsurface initiated atom transfer radical polymerization (ATRP) from the initiator moieties incorporated in the stiff hydrogel constituting the bulk of the substrate. Firstly, a solution containing monomers of acrylic acid (AAc) and acrylamide (AAm), crosslinker of N,N'-methylene bis(acrylamide) (BIS), radical initiator of potassium persulfate (KPS), accelerator of N,N,N,N-tetramethyldiamine (TEMED) and ATRP initiator monomer 2-(2-bromoisobutyryloxy) ethyl methacrylate (BrMA), was poured into a glass mold to carry out free radical polymerization at room temperature for 12 h. Poly (AAm-AAc-BrMA) hydrogels embedded with ATRP initiator, named Hy-Br, were obtained. The Hy-Br were soaked in Fe^{3+} solution for 24 h to allow second physical crosslinking, resulting in the high-strength hydrogel HHy-Br.

Then, the HHy-Br samples were immersed into degassed monomer solution to perform the ATRP from the sub-surface. Typically the zwitterionic poly(2-(methacryloyloxy) ethyl) dimethyl-(3-sulfopropyl) ammonium hydroxide (PSBMA) and anionic poly(3-sulfopropyl methacrylate potassium (PSPMA) polymer brushes were chosen to modify the HHy-Br substrate. When polymerization proceeds, the grafted brushes diffuse into the hydrogel, which exposes more initiator to the monomer solution, leading to a grafting polymerization to penetrate down into the sub-surface. PSBMA and PSPMA brushes interlocked into HHy-Br, resulting in bi-layered hydrogels HHy-g-PSBMA and HHy-g-PSPMA, respectively.

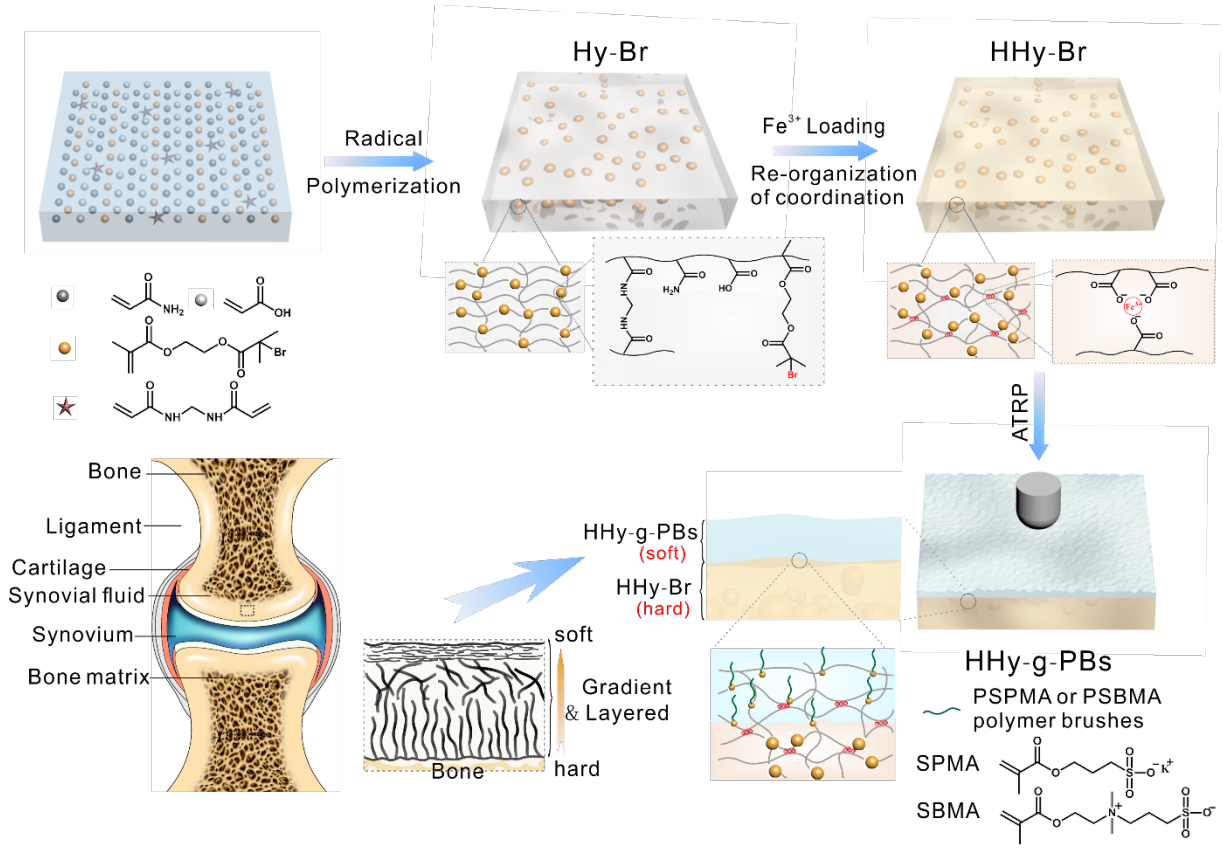

Figure 1. Ideation of cartilage-like hydrogel. Schematic illustration for the fabrication procedures of PSPMA or PSBMA brushes-grafted hydrogels. The high strength hydrogel substrate with BrMA embedded was fabricated by radical polymerization and post-treatment with ferric ions. Subsequently, the layer of polymer-brushes-grafted-hydrogel (HHy-g-PBs) was prepared by the ATRP method at the sub-surface. The composite configuration, combining the soft HHy-g-PBs layer with a strong HHy-Br substrate, was designed to best mimic the structure of articular cartilage.

The material was characterized by FT-IR spectra (Figure S1) and X-ray photoelectron spectroscopy (XPS) (Figure S2-S3). The asymmetrical stretching vibration signals at 1737 cm^{-1} found on both FT-IR spectra of Hy-Br and HHy-Br samples were ascribed to the C=O bond of ester groups, and further confirmed the presence of BrMA in hydrogels. The carbonyl signal on HHy-Br was weaker than that in the Hy-Br spectrum, due to the attenuation caused by the ionic coordination between Fe^{3+} and COO^- (Figure S1). As shown in Figure S2, compared with

pure hydrogel (HHy), the appearance of the Br3d peak at 70 eV indicated the successful entanglement of the ATRP initiator in the network of Hy-Br and HHy-Br. In XPS fine spectra, the characteristic K2p peak at 293 eV and S2p peak at 168 eV clearly demonstrated the successful grafting of PSPMA polymer brushes at the interface with HHy-Br, and the N1s peak showed shift (400.2 eV) after grafting PSBMA brushes compared with the other four spectrums (399.6 eV), which was attributed to the appearance of ammonium N^+ on PSBMA side chains (Figure S3).

2.2. Characterizations of bi-layered composite hydrogel

The morphology and grafting kinetics were studied using the HHy-Br matrix with 5 wt% BrMA content. Figure 2(a-b) shows the change of surface pattern of HHy-g-PSBMA and HHy-g-PSPMA top layers along with the polymerization time. The wrinkling patters grew as soon as grafting started, while the size of wrinkles (thus the surface roughness) became increasingly larger by extending the polymerization time from 5 min to 120 min. The physical mechanism originating the wrinkling is the different hydration capability of the top layer and the bulk hydrogel, resulting from their different elastic properties. As speculated, the wrinkling patters on the top surface of the layered material can be used to store lubricant and reduce the contact area. Tracking the morphology evolution showed much faster growth kinetics for PSPMA than PSBMA, as shown from the growth kinetics vs. polymerization time curves in Figure 2c. The thickness of the resultant top layer can be finely controlled by the polymerization time.

The SEM gives a more clear insight in morphology differences for both HHy-g-PBs sample. Taking layered samples with the polymerization time of 40 min as an example, the HHy-g-PSPMA shows randomly distributed clusters with separation of 10~20 μm and apparently irregular textures within a single cluster (Figure 2d). Inside each cluster a reduced porosity appears, with an overall top layer at almost constant thickness of ~53 μm (Figure 2d). By contrast, the surface of HHy-g-PSBMA sample exhibited a cobblestone-like grid structure

with larger porosity (Figure 2e); furthermore, the thickness of the top layer was ~18 μm (Figure 2e). As expected, mesh textures or dense small pores on the top layers of the composite can be extremely beneficial for maintaining and binding a water layer during squeeze-out contact dynamics.[12]

The mechanical strength of the HHy-Br samples (substrate material) was measured on a universal mechanical testing machine. Taking a HHy-Br sample with 5% BrMA concentration as an example, a typical tensile stress-strain and compressive stress-strain curves are presented in Figure 2(f-g). The tensile stress of HHy-Br hydrogel can reach as high as 12 MPa at a strain of 161% (Figure 2f), while its compressive stress reached ~15 MPa even when only compressed to 31 % (Figure 2g). Correspondingly, the calculated elastic modulus both in tensile and compression mode is ~40 MPa with considering a strain range of 0~10% . The results showed that the bottom HHy-Br hydrogel layer can potentially bear high contact pressure. It is observed that, after surface grafting, the mechanical properties of the bulk do not significantly change.

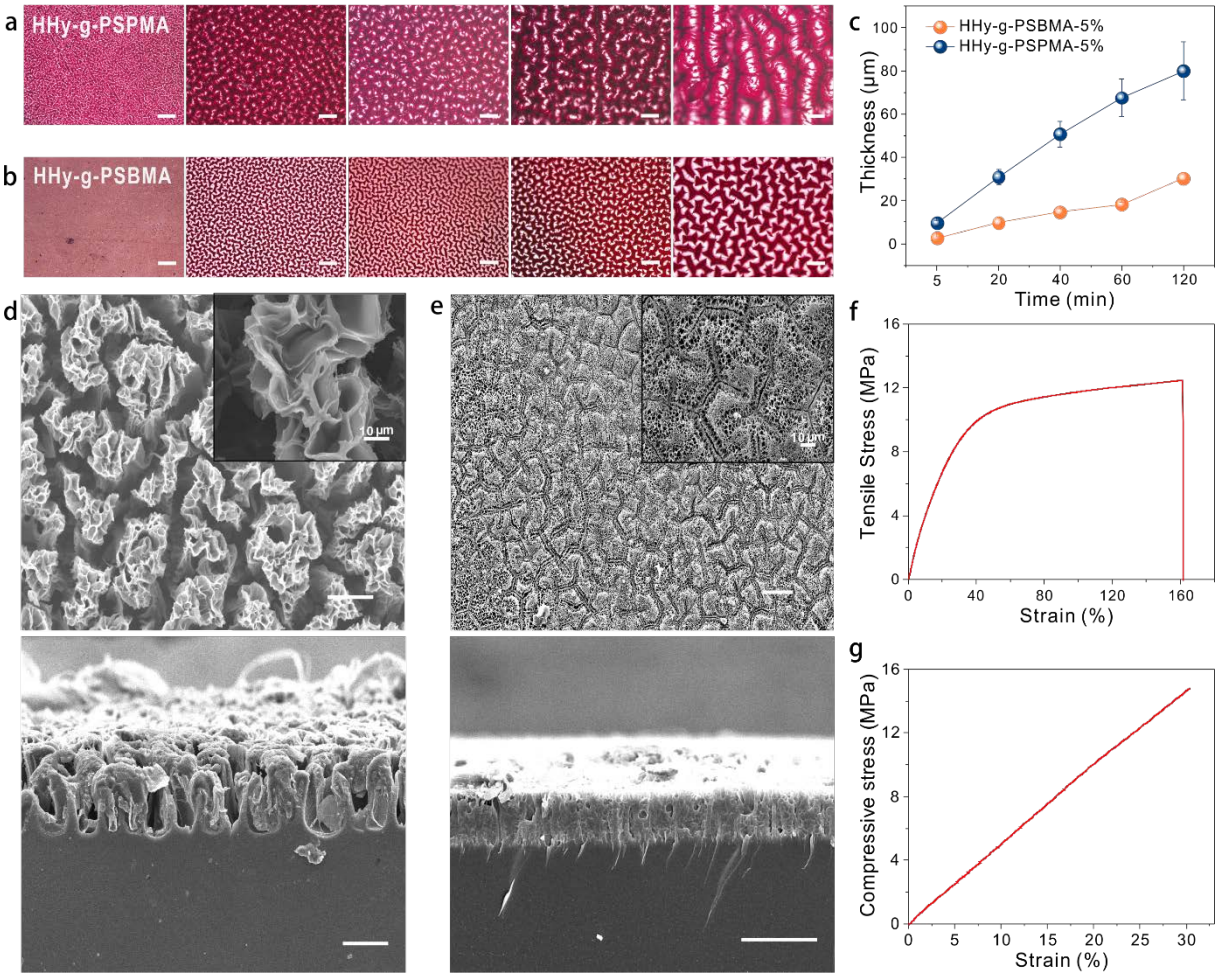

Figure 2. Growth kinetics of HHy-g-PBs top layer. The optical images show the surface morphologies evolution generating the top HHy-g-PBs layer upon grafting PSPMA (a) and PSBMA (b) polymer brushes at increasing polymerization time from 5 min to 120 min (scale bar: 100 μm). (c) The thickness change of the top HHy-g-PBs layer with polymerization time. SEM images showing the surface and cross-sectional morphologies for layered HHy-g-PSPMA sample (d) and layered HHy-g-PSBMA sample (e) (scale bar: 50 μm), and magnified acquisition in the inset (scale bar: 10 μm). (f) The typical tensile stress−strain curve of HHy-Br hydrogel. (g) Compressive stress−strain curve of HHy-Br hydrogel.

2.3. Evaluation of the lubrication property of bi-layered composite hydrogel

The lubrication property of the hydrogel composite samples was investigated with a reciprocating ball-on-disk tribometer, where steel balls with 6 mm diameter and roughness of

20 to 50 nm (root mean square roughness) were used as friction counter-pairs. Compared with friction property of bare sample without chemically grafting (Figure S4), surface grafting polymer brush would significantly reduce the COFs. Firstly, it was found that the change of initiator moiety BrMA concentration had a reduced effect on the lubrication property, with the COFs roughly around 0.010 (Figure S5). On the opposite, the hydrated layer thickness, ruled by the polymerization time, had a strong impact on the COFs. At the polymerization time of 40 min, both samples could achieve the lowest COFs (Figure 3a and Figure 3b). The low COFs of both samples can be attributed to the synergistic effect of high hydration of charged PSPMA and PSBMA brush chains embedded in the HHy-g-PBs composite layer and the water-based weeping of thin hydrogel films.[13] Up to 120 min polymerization time, all the HHy-g-PSBMA kept small COFs (the thickness of the top layer of HHy-g-PSBMA slowly increases with the polymerization time, up to about 30 μm in the experiments), while the COF of HHy-g-PSPMA (the thickness of the top layer reached 80 μm) increased significantly to 0.026. This may be attributed to the large thickness which induces an increase of viscoelastic drag[5e] as well as an increased true contact area (see Discussion section), the latter determining a larger adhesive contribution to the total frictional stress.

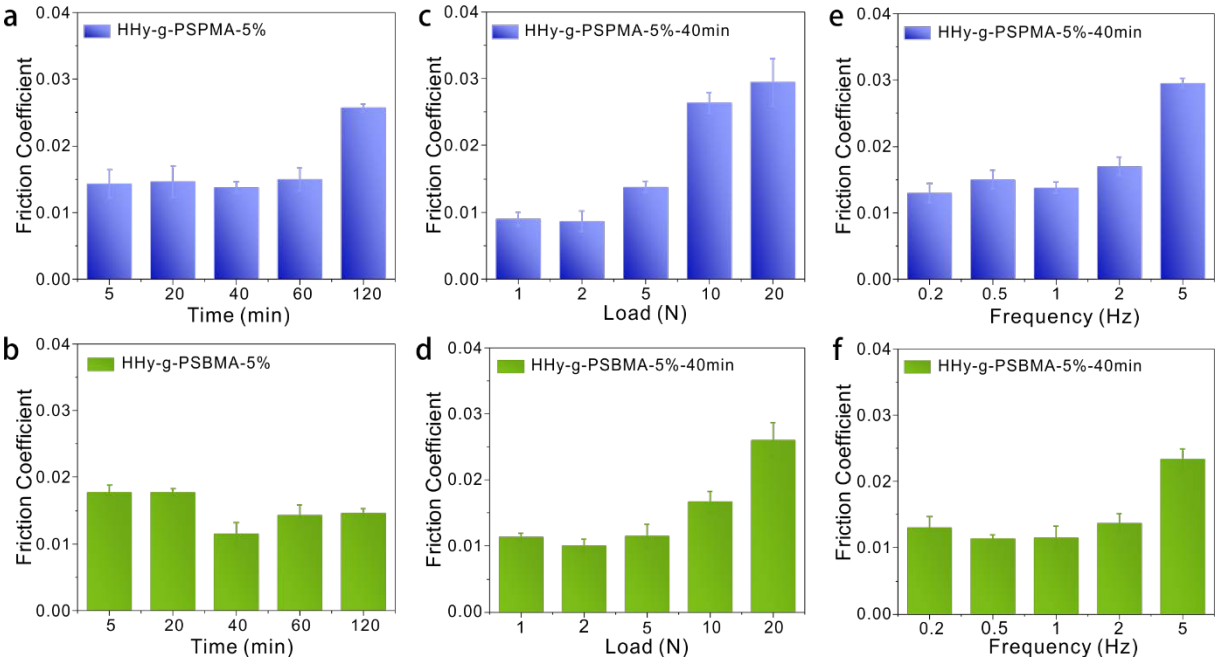

Figure 3. Evaluation of lubrication behavior of both HHy-g-PBs samples. COFs of (a) HHy-g-PSPMA and (b) HHy-g-PSBMA obtained with different polymerization times (frequency at 1 Hz, the load of 5 N). COFs of (c) HHy-g-PSPMA and (d) HHy-g-PSBMA under different loads (polymerization time at 40 min, frequency at 1 Hz). COFs of (e) HHy-g-PSPMA and (f) HHy-g-PSBMA at different frequencies (polymerization time at 40 min, the load of 5 N). The concentration of BrMA initiator in all the samples above was 5 wt%, the lubricant was water and friction pairs were smooth (20 to 50 nm rms roughness) steel balls with a diameter of 6 mm.

The effect of applied loads on the COFs of the HHy-g-PBs samples was also experimentally investigated. As shown in Figure 3c and 3d, increasing the load from 1 N to 20 N resulted in an increase of COFs from 0.009 to 0.030 for HHy-g-PSPMA and from 0.011 to 0.026 for HHy-g-PSBMA. The maximum Hertz contact pressure (P_{max}, assuming the composite to be constituted by the bulk slab only, with infinite thickness) in such range of loads was calculated, as shown in Table S1. P_{max} was ~ 3.97 MPa at 1 N and ~ 10.8 MPa at 20 N, matching closely the typical values found in cartilaginous joints.[4b] Specially at applied loads of 1~2 N, both HHy-g-PSPMA and HHy-g-PSBMA samples exhibited ultralow COFs (around 0.010). The COFs for these two samples increased noticeably when the normal loads increased from 2 N to 20 N. This is due to the increased indenter penetration depth and, consequently, increased viscoalestic drag with applied load, as expected because of a poroelastic response of the system (see Discussion section). The COFs were also impacted by the sliding frequency (Figure 3e and 3f). Slight fluctuations of COFs were observed in the frequency range from 0.2 Hz to 2 Hz, whilst the value of the COFs increased at a frequency of 5 Hz. This can be explained by noticing that the hydrated lubrication layer is affected by the speed at which water replenishes the contact and, at larger speeds, a different equilibrium of fluid flow is reached corresponding to less water being available for weeping into the contact.

2.4. Evaluation of the long-life wear resistance of bi-layered composite hydrogel

The robustness of the bi-layered materials was tested with a set of long-life wear experiments (10k cycles) at relatively high loading conditions. As shown in Figure S6, during the 10k sliding cycles, the COFs of the layered HHy-g-PSPMA sample were considerably constant to a low value both under the normal loads of 5 N (P_{max} ~6.78 MPa, COF ~0.014) and 10 N (P_{max} ~8.55 MPa, COF ~0.016). However, it was observed that COF increased gradually with the cycle number at normal loads of 20 N (P_{max} ~10.7 MPa), yet without exceeding 0.060. Similarly, for the HHy-g-PSBMA samples the COF was varying between ~0.020 (at 5 N, P_{max} ~6.78 MPa) and ~0.024 (at 10 N, P_{max} ~8.55 MPa) for loads in the range 5 to10 N, again with negligible dependence on the number of cycles. The case at 20 N applied load showed a limited COF increase to values lower than ~0.050 (P_{max} ~10.77 MPa) (Figure S7).

In some cases, the long-life wear tests were extended up to 50k sliding cycles, as shown in Figure 4a for a normal load of 10 N. The COF of the HHy-g-PSPMA sample was stable at ~0.025 during the entire 50k cycles. On the opposite, the COF of the HHy-g-PSBMA sample increased slowly and finally remained constant value of ~0.050 after 50k sliding cycles (Figure S8), demonstrating the capability of the synthetic cartilage to preserve the weeping and lubricity mechanisms upon many-cycles rubbing. Then, the surface morphology of the samples after friction test was evaluated. As shown in Figure S9, surface scar at the sliding area for bare sample without brush grafting was clearly observed only after 3500 sliding cycles. Subsequently, after 50k sliding cycles, the surface morphologies of both layered samples were observed, Figure 4b. To improve the accuracy of the optical acquisition, the sliding contact area was stained with dyes for cross-sectional epifluorescence imaging. A depression (depth: ~60.42 μm; width: 1087.00 μm) was observed for the contact area while the light red fluorescence layer indicated the persistence of the top lubrication layer (Figure 4b_1). Aligned wear scratches were identified at the sliding contact area both from the optical microscope (Figure 4b_2) and the SEM characterization (Figure 4b_3, marked as *n*), compared with the non-contact region

(Figure 4b$_3$, marked as *m*). However, the SEM magnified acquisitions indicated that the very well delineated texture of the top HHy-g-PSBMA lubrication layer was only marginally affected by contact with the sliding counter-surface after 50k sliding cycles (Figure 4b$_4$). Similarly, a depression (depth:~94.93 μm; width: 1530.00 μm) with a neat red fluorescence layer was also observed for the HHy-g-PSPMA sample (Figure 4c$_1$), while almost no wear scratches were identified at the sliding contact area (marked as *k*) (Figure 4c$_2$-4c$_4$), indicating the robustness and excellent wear-resistance of the top HHy-g-PSPMA layer, as well as the remarkable capability to increase the degree of conformity with the rigid indenter surface (leading to a reduced contact stress, see also Discussion section), see Figure 4d. Furthermore, compared with traditional systems with polymer brushes grafted only via a single chemical linkage,[14] the polymer brushes in the current system were chemically embedded into the network of high strength hydrogel, which endows them considerable resistance contact and shear stresses.

As analyzed, our system provides, for the first time, the missing link between hydrogel- and polymer brushes-based lubrication in order for the two low-friction mechanisms to be extended to macroscale applications, such as for the natural system. Indeed, whilst on one side polymer brushes alone show a limited capacity of supporting high loads at macroscale with rough surfaces, on the other side hydrogels mimicking cartilage are typically unlikely to provide, simultaneously, low friction, high load-bearing and wear-resistance capacity, see Table S2.

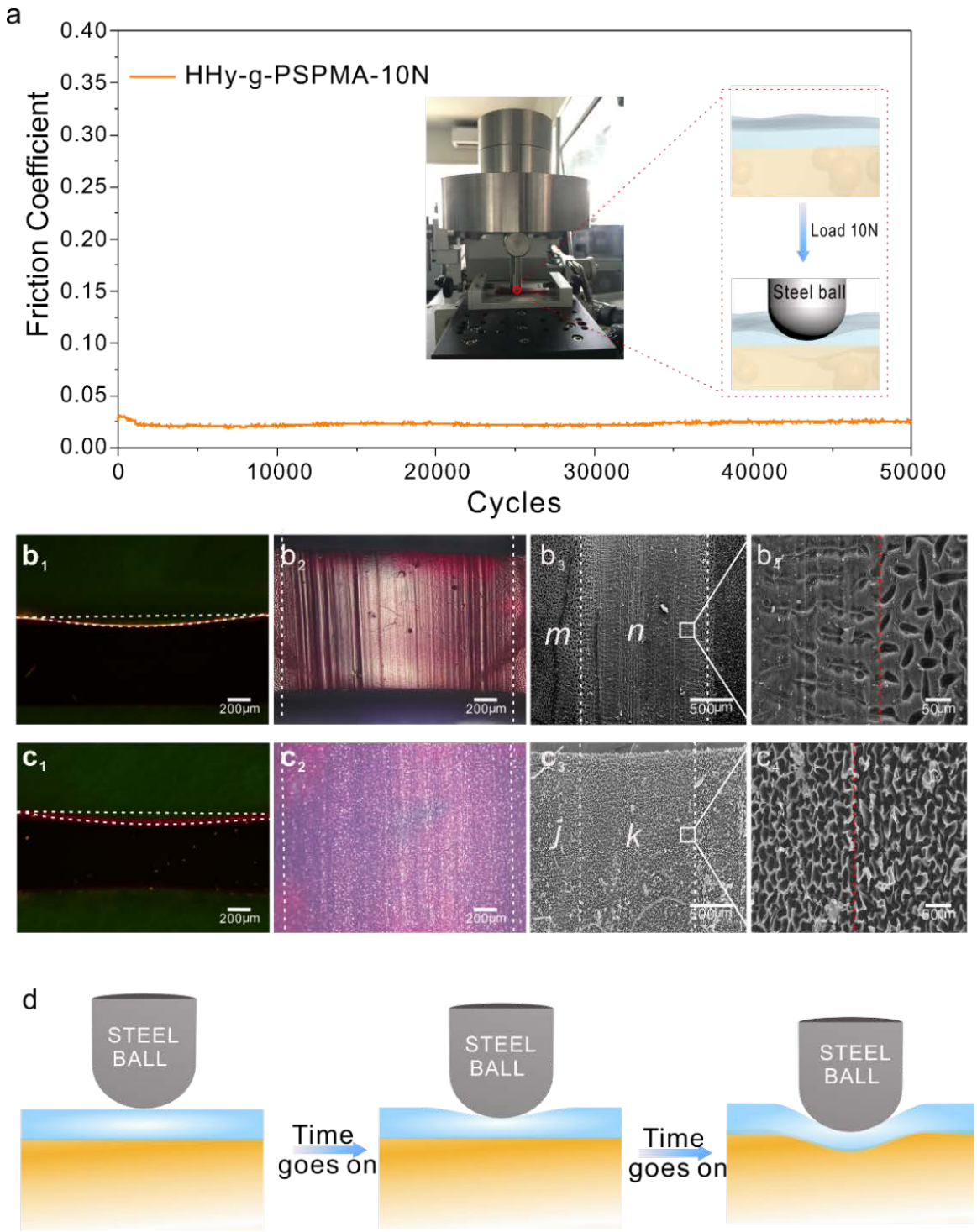

Figure 4. Evaluation of lubrication persistence and wear-resistance of the layered samples. (a) The COF curve of HHy-g-PSPMA for 50k sliding cycles under a normal load of 10 N at a frequency of 1 Hz. The wear characterization for (b) HHy-g-PSBMA and (c) HHy-g-PSPMA samples separately upon encountering 50k friction sliding cycles: (b_1 and c_1) the cross-sectional fluorescence imaging of sliding contact area, (b_2 and c_2) the surface optical microscope top view of sliding contact area, (b_3 and c_3) the SEM images showing the morphologies of sliding

contact (marked as *n* and *k*) and non-contact (marked as *m* and *j*) areas and (b_4 and c_4) the SEM magnified acquisitions. (d) The schematic diagram showing the evolution process from the non-conformal to a higher degree of contact conformity of the layered HHy-g-PSPMA sample.

3. Theoretical analysis and models

Lubrication by polymer brushes was reported as early as in 2003, where it was shown that end attached polystyrene brushes can provide extremely low friction due to steric repulsion between free ends.[12] Since then, aqueous lubrication with ultralow friction was achieved by hydrophilic polymer brushes on atomically flat substrates (mica) within surface force apparatus.[10] Nevertheless, in macroscale test level such as for in-vivo applications, nano-thin polymer brushes are liable to be torn even under small loading because of the existing roughness of the sliding pair.[15] This is already the case of a smooth hard artificial joint grafted with zwitterionic polymer brushes, which hardly showed an ultra-low coefficient of friction in realistic contact conditions because of the high contact stresses (proportional to $E^{2/3}$, where E is the Young's modulus), which could not be avoided even with the adopted smooth surfaces.[14] Therefore, in the worst case of rough or wear-induced roughened hard mating surfaces, which typically results in a wider (than in the Hertzian case) distribution of interface contact stresses (due to the multiscale fragmentation of the nominal contact into micro- to nano-scale contact patches), polymer brushes alone on a rigid substrate cannot represent a good candidate to provide ultralow friction. Indeed, the adoption of polymer brushes on a rigid substrate does not fully mimic the natural articular cartilage, whose elastic and, thus, hydration properties are graded continuously across the depth from the contact surface.

To gain further insights on the effect of graded elasticity on the behavior of our system, the sliding contact between the layered material and the spherical indenter was modeled recurring to a two-scales contact mechanics model (Figure S10), formulated in boundary lubrication. Indeed, the thickness of the hydrated layer (typically larger than ~ 10 μm, see SEM

cross-sections in Figure 2d to 2e) and the relatively large roughness of the top layer (e.g. with a root mean square roughness comparable with the layer thickness for the HHy-g-PSPMA composite) fully prevent the contact to operate under either mixed or full film lubrication, as suggested recently by some of us.[5e] Thus, in our system the friction originates from an adhesive contribution, which is linearly proportional to the amount of true solid contact area between the indenter and composite lubrication layer, as well as from the dissipation resulting from the hydrogel contact-induced weeping dynamics, occurring within the top lubrication layer. The latter acts on a time scale which is estimated to be $\tau_{\mathrm{r,gel}} \approx 1$ ms in our system.[5e] Thanks to the large separation of length scales between the largest roughness wavelength and the nominal contact radius (of order of the Hertzian contact radius), the true contact area, i.e. the total contact area between the spherical indenter and the rough composite top layer (responsible for the adhesive contribution to friction), will then be (approximately) determined by separately solving the smooth macroscale contact mechanics from the rough contact mechanics as shown in Supplementary Section S2.

In Figure 5 we report a comparison between theoretical predictions and experimental results. In particular, in Figure 5(A) we show the results of a parametric investigation of the contact mechanics occurring in our system, in order to disclose the interaction fundamentals. In the parametric investigation, the top layer thickness is varied in the range from 1 to 100 μm. The sliding speed is varied in the range of 1 mm/s to 100 mm/s accordingly to the experiment (stroke length 10 mm). In Figure 5(A.1) we show the three-dimensional representation of the contact area and pressure formation at the macroscale sliding contact. In particular, the indentation on the highly hydrated lubrication layer determines the occurrence of pile-ups located at the outer edges of the contact area, leading to a larger degree of contact conformity with respect to a classical Hertzian interaction, reducing therefore the maximum contact pressure. The effective solid contact pressure distribution is qualitatively similar to the Hertzian distribution, with relatively small dependence on the weeping relaxation time for the thin

composite lubrication layer (see also Figure S11 for other top layer thicknesses). In Figure 5(A.2) the nominal contact area A0 (i.e. the contact area obtained in the ideal case of smooth layered material) as a function of the normal load F_N is reported for different values of the hydrated layer thickness. The dependence with the sliding speed (not shown here) can be neglected in the range of velocities adopted in our system, apart for the larger speed (100 mm/s), where the hydrogel effective viscoelasticity do affect the contact area formation at the macroscale (Figure S11), in line with experiments. Figure 5(A.3) shows the contact area formation at the roughness scale. In particular, the normalized contact area as a function of the nominal (locally averaged) squeezing pressure is reported for different values of hydrogel top layer thickness and root mean square roughness. At the roughness scale, the dependence with the sliding speed is always negligible for our system.

Figure 5B reports the comparison between the measured and theoretically predicted friction as a function of squeezing load. In particular, in Figure 5(B.1) we show the true solid contact area as a function of the squeezing load, as obtained for the system adopted in Figure 5A (with sliding speed 10 mm/s and hrms=10 μm). Note that, for small coating thickness, the introduction of roughness in the contact determines a strong reduction in the true contact area between the indenter and the top layer (compare Figure 5(A.2) with 5(B.1)) with respect to the ideal smooth case. In Figure 5(B.2) we finally report the comparison between the friction predicted by the two-scales contact model and the experimental results for both the HHy-g-PSBMA (red curves) and HHy-g-PSPMA (black). In the theoretical results, only the adhesive contribution to friction is computed, with the true shear stress τ assumed to be pressure independent and comparable to the elastic modulus of the hydrated layer, i.e. $\tau \approx 20$ kPa. Furthermore, in the comparison, we have assumed the HHy-g-PSBMA with 20 μm thickness and 10 μm hrms, whereas for the HHy-g-PSPMA the thickness is 50 μm and the roughness is 50 μm. The sliding speed is 10 mm/s. We observe the general good qualitative agreement with the experimental data, where the difference with the experiments has to be ascribed to the

dissipation contribution coming from the hydrogel contact-induced weeping dynamics occurring in the hydrated (viscoelastic) layer. Indeed, in order to achieve a better prediction of the frictional properties of the hydrogels under consideration here, one needs to consider the viscoeleastic response of the system and include a hysteretic sliding friction approximately given by $\mu_{\mathrm{hys}} \approx \alpha \tan\delta p_0/\mathrm{E}_0$, where p_0 is the average indentation pressure, $\tan\delta$ is the loss tangent and α a geometric prefactor of order one.[5e] In our system $\tan\delta \approx \omega\tau_{\mathrm{r}}$, leading to $\mu_{\mathrm{hys}} \approx \omega\tau_{\mathrm{r}} p_0/\mathrm{E}_0$. As an example, for small loads $p_0 \sim \mathrm{E}_0$ (see the dependence with the squeezing load in Figure S12) so that $\mu_{\mathrm{hys}} \approx \omega\tau_{\mathrm{r}}$, leading in our system to $\mu_{\mathrm{hys}} \approx 10^{-2}$ order of magnitude (considering $\tau_{\mathrm{r}} \approx 10^{-3}$s and $\omega = \pi v_0/a_{\mathrm{c}} \approx 10 s^{-1}$), in qualitative agreement with the experimental findings. The estimation of the bulk dissipative contribution relies on the accurate evaluation of the visco-poroelastic properties of the composite hydrogel lubrication (top) layer, which will be the subject of a separate dedicated contribution.

We stress that, because of the folding mechanism which determines most of the surface roughness in our system, the root mean square roughness in the real system scales approximately with the top layer thickness, as typically in surface wrinkling formation processes. However, increasing the roughness and the thickness of the compliant layer have opposite (compensating) effects on the contact formation, and this qualitatively explains the friction behavior which is relatively similar in the HHy-g-PSPMA and HHy-g-PSBMA samples, despite of the different micro-geometrical properties of their top layers. From simple contact mechanics arguments, assuming the local rough contact mechanics to occur under relatively small values of normalized true contact area, one can easily show that the local average squeezing pressure $\sigma_0 \propto \mathrm{E} \cdot \exp(-\mathrm{u}/\mathrm{h}_{\mathrm{rms}})$, where u is the locally averaged interface separation and E an equivalent elastic modulus which takes into account of the composite nature of the hydrogel (it decreases by increasing the top layer thickness t, in the simplest qualitative picture $\mathrm{dE}/\mathrm{E} \propto -\mathrm{dt}/\mathrm{t}$). Thus, a same average interface separation between two systems is

obtained when the contact pressure is varied accordingly to $d\sigma_0/\sigma_0 \approx dh_{rms}/h_{rms} - dt/t$, where $d(\cdot)$ corresponds to the variation of the generic physical property $(\cdot)$. Since $h_{rms} \sim t$ in our composites, the scaling above suggests that the contact mechanics and the friction occurring in the HHy-g-PSPMA and HHy-g-PSBMA systems are bound to be qualitatively similar, in agreement with the theoretical and experimental findings of Figure 5B.

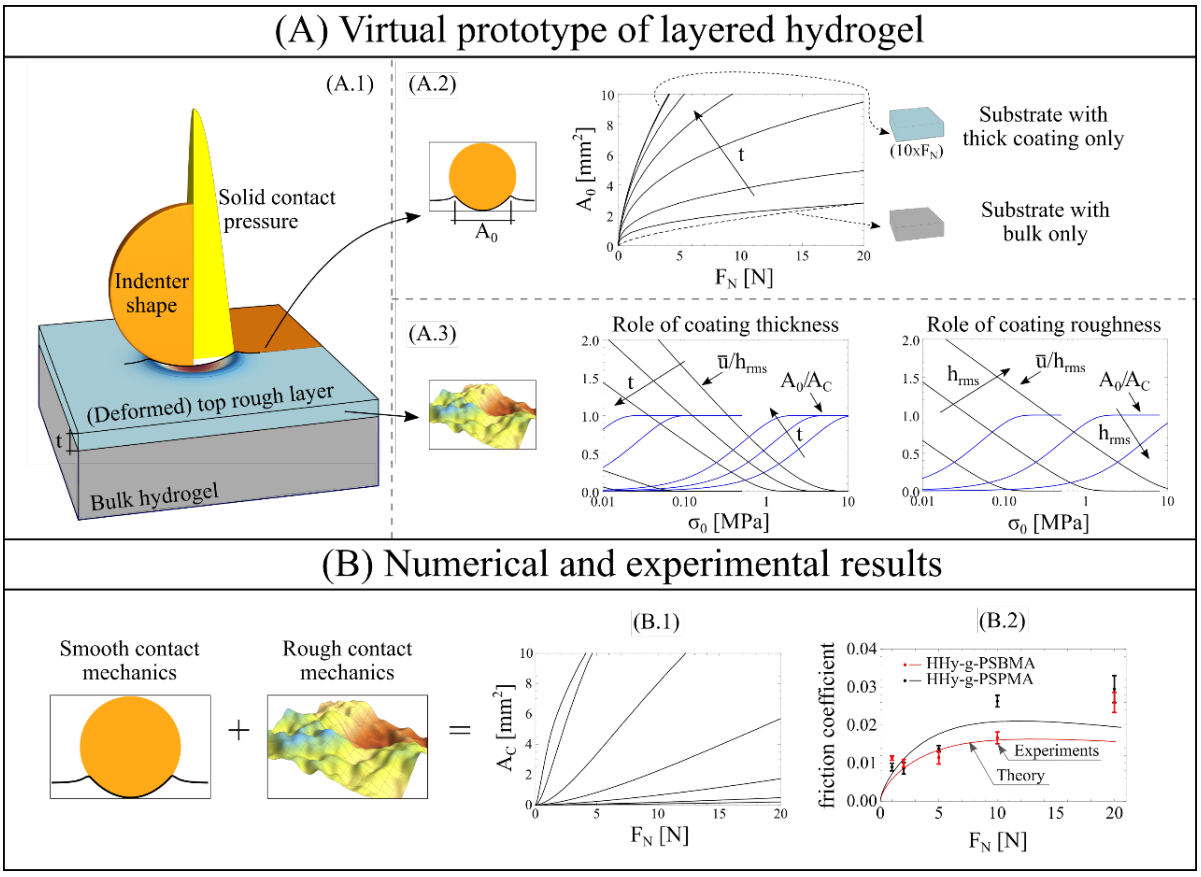

Figure 5. Theoretical Results and Comparison with Experiments. (A) Virtual prototype of hydrogel composite in sliding contact with the spherical probe, and corresponding numerical results. (A.1) Three-dimensional representation of the contact area and pressure formation at the macroscale sliding contact. (A.2) The nominal contact area A0 as a function of the normal load FN is reported for different values of the hydrated layer thickness. (A.3) The normalized contact area as a function of the nominal (locally averaged) squeezing pressure is reported for different values of coating thickness and root mean square roughness. (B) Comparison between the measured and theoretically predicted friction as a function of squeezing load. (B.1) True solid contact area as a function of the squeezing load (reported for different values of the

hydrated layer thickness) and (B.2) friction coefficient for both the HHy-g-PSBMA (red curves) and HHy-g-PSPMA (black). In the theory, only the adhesive contribution to friction is included.

The experimental results presented above demonstrate that the two-layers graded hydrogel composite show friction performances comparable with the natural articular cartilage, despite of the simplified architecture. Indeed, the macroscopic deformation response of the natural tissue is dictated by the biphasic nature of the material, and the exceptional lubrication can be ascribed to the flow-dependent (weeping) and flow-independent (due to the solid matrix) viscoelasticity of its constituent,[16] coupled with the exceptional boundary lubricating properties of lubricin.[17] In our material, for the first time, the hydrogel substrate provides the loading support, while the top layer provides the brush- and weeping-lubrication mechanisms. The latter, however, needs to be accurately designed as it might also unnecessarily increase the viscoelastic dissipation, thus the perceived friction, in the system. It is, therefore, to be expected that increasing the load (or the thickness and/or structure of the lubricating layer) affects the mechanical response of the system, with increased deformation corresponding to more viscoelastic losses in either the surface layer or the substrate, less fluid support and larger stresses in the solid matrix. The overall response is indeed dependent on a number of geometric and test parameters (stroke length, frequency, load). However, this may not necessarily correspond to the alteration of the brush-lubricating properties of the surface layer, which can be considered contact pressure-independent in the conditions studied here. The deformation of the system might or may not be permanent depending on the applied load and the time left for material re-imbibition and swelling, as well as physical alteration of the sample. Permanent deformations can be induced by high loads, which in turn may lead to a visco-plastic material response.

4. Conclusion

Inspired by the typical layered biochemical features and the surface lubrication mechanism of articular cartilage, a novel layered material with high load-bearing, low friction and wear-resistance performances has been designed, made and tested. A robust polymer brushes-grafted hydrogel (HHy-g-PBs) composite is generated by chemically embedding hydrophilic polyanionic PSPMA brushes or the polyzwitterionic PSBMA brushes into the sub-surface of the high strength hydrogel with the ATRP initiator (HHy-Br). The as-prepared layered material shows a stable low-friction property (COF<0.025) under an extreme harsh test condition (max Hertz contact pressure 8.5 MPa), by only employing low viscosity water as lubricant. In particular, the COF can remain at a low level even under 10 MPa contact pressure. The lubrication property of the layered material is highly related to the mechanics of bonding of the grafted PSBMA or PSBMA polymer brushes, which is highly dependent on the ATRP initiator concentration and the polymerization time of the brushes. The synergy between the robust HHy-g-PBs composite lubrication layer, which provides excellent aqueous lubrication due to the mechanisms illustrated theoretically above, and high strength HHy-Br hydrogel layer, which gives load-bearing capacity, is responsible for realizing its high load-bearing and low friction properties. Moreover, compared with traditional polymer brushes-modified surfaces, the hydrophilic polymer brushes on the surface of our layered material are entangled into the high strength hydrogel network, which allows them to resist the mechanical sliding-induced shear stresses. As a result, almost no wear was observed on the surface of the composite lubrication layer of the HHy-g-PSPMA sample after 50k sliding cycles under 8.5 MPa contact stress, which exceeds physiological stresses experienced by articular cartilage. Overall, this bi-layer hydrogel design, inspired by nature provides a new route for the development of excellent water lubrication materials.

5. Experimental Section

Materials: 2-Hydroxyethyl methacrylate (HEMA, 99%), 2-bromoisobutyryl bromide (98%) and [2-(Methacryloyloxy) ethyl] dimethyl-(3-sulfopropyl) ammonium hydroxide (SBMA) were purchased from J&K Chemical Ltd and used as received. Acrylic acid (AAc), acrylamide (AAm), N,N'-Methylenebis (acrylamide) (MBAA) and N,N,N,N-tetramethyl ethylene diamine (TEMEDA) were purchased from Sigma-Aldrich, and ammonium persulfate (APS), iron chloride hexahydrate ($FeCl_3 \cdot 6H_2O$), sodium carbonate (Na_2CO_3) and sodium chloride (NaCl) were purchased from Sinopharm, China. Dichloromethane and anhydrous methanol were purchased from Tianjin Chemical Reagents Corp. Dichloromethane was dried over CaH_2 before use. 2,2'-bipyridine (Bipy, 99%), copper (I) bromide (CuBr) and 3-Sulfopropyl Methacrylate Potassium (SPMA) were purchased from TCI Co., Ltd. CuBr was purified by stirring overnight in acetic acid.

A mixture solution of HEMA (11.45 g, 0.088 mol) and triethylamine (4.05 g, 0.04 mol) in dichloromethane (45 g, 0.53 mol) in a flame dried round-bottom flask was cooled to 0 ℃ in an ice bath under nitrogen atmosphere for 20 min. Subsequently, 2-Bromoisobutyryl bromide (18.393 g, 0.08 mol) in dichloromethane (23.25 g, 0.274 mol) was added dropwise to the mixture solution. The resulted solution was stirred at 0 ℃ for 4 h to complete the reaction. The white precipitate was filtered off and washed with dichloromethane twice. The liquid was collected and washed respectively with saturated Na_2CO_3 and saturated NaCl for several times until the solution pH was at about 7. Finally, the solvent was evaporated and the crude product was purified by column chromatography, resulting in a pale yellow liquid.

Synthesis of Tough HHy-Br Hydrogel: The tough P(AAc/AAm) hydrogel with ATRP-Br initiator (P(AAc/AAm)-Br hydrogel) was synthesized via two steps. First, monomer of AAm (6.5 g, 0.09 mol) and AAc (1.625 g, 0.0226 mol), initiator of APS (1 wt% of monomers), crosslinker of MBAA (0.03 mol % of acrylic acid and acrylamide), HEMA-Br initiator different mass ratios (0.5 %, 1 %, 2.5 %, 5 %, 10 % mass ratios of HEMA-Br/AAm) and accelerator of

TEMED (40 μL) were added in 30 mL pure water to obtain homogeneous solution. After vigorously stirred for 1min with gassing nitrogen, the resulting solution was poured in a glass mold and placed at room temperature overnight to form a covalently cross-linked hydrogel. Then the covalently cross-linked hydrogel was immersed in the Fe^{3+} solution (0.25 mol/L) for 24 h to form the secondary ionic crosslinking network. Finally, the hydrogel was immersed in deionized water for 48 h to remove superfluous Fe^{3+}.

Synthesis of PSPMA and PSBMA Brushes Grafted Hydrogels (HHy-g-PBs): Polymer brushes were grafted from initiator embedded P(AAc/AAm)-Fe^{3+}-Br hydrogel substrate by atom transfer radical polymerization (ATRP) technique. The typical polymerization process is as follows. The monomer was dissolved in the water/methanol at room temperature and degassed for 30 min with N_2 steam. And then the Bipy and CuBr were added in this solution in the Schlenk tube successively. The mixture was further stirred and degassed with N_2 for another 20 min. The P(AAc/AAm)-Br hydrogel sheet with one side protected by 3 M tape was put into the reaction solution in the U-TYPE tube under N_2 protection without stirred for a certain period (5, 20, 40, 60, 120 min). Finally, the samples were taken out and washed with deionized water to remove any unreacted monomers and catalysts. The corresponding recipes for the two polymers to polymerize are as follows: water 8 mL, methanol 4 mL, SPMA 6 g, bipy 80 mg, CuBr 35 mg; water 8 mL, methanol 4 mL, SBMA 6 g, bipy 180 mg, CuBr 60 mg.

Mechanical Characterization of HHy-Br Hydrogel: An electrical universal material testing machine with a 500 N load cell (EZ-Test, SHIMADZU) was used to perform the tensile and compressive tests of HHy-Br hydrogels. The samples were cut into rectangular shapes (length: 50 mm; width: 3 mm; thickness: 1 mm) for tensile tests and square shapes (length: 3 mm; width: 3 mm; thickness: 1 mm) for compressive tests. The crosshead velocity was kept at 100 mm/min for tensile tests and 0.1 mm/min for compressive tests. The elastic modulus both in tensile and compression mode is calculated by recording the slopes with considering a strain

range of 0~10%, at least three parallel tests were performed to obtain the average value. All the specimens were coated in silicone oil during the tests.

The Morphology Characterization: The scanning electron microscope (SEM, JSM-5600LV at an accelerating voltage of 20 kV) and optical microscope Olympus BX51 were employed to observe the surface morphology of samples. The samples for SEM tests were frozen in the atmosphere of liquid nitrogen for 10min, and then gotten dried at -40 °C in 1 Pa for 24 h by freeze-drying method.

The Elements Characterization: An FT-IR spectrometer (Nicolet iS10, Thermo Scientific, USA) was employed to assess the chemistry components of original tough layered hydrogels. Subsequently, the polymer brushes grafted layers of HHy-g-PBs were also characterized by ATR-IR.Further, the surface chemistry components of samples in different synthesis steps were also characterized by XPS using a Thermo ESCLAB 250Xi spectrometer with a monochromatic Al Kα radiation. Meanwhile, the C1s line at 284.6 eV from adventitious carbon was used as a reference.

The Growth Kinetics Characterization: After the samples immersing in pure water until equilibrium, the samples were stained with Rhodamine B (1 mg/mL) for 10 min and imaged the fluorescent cross-section of samples to observe the thickness of polymer brushes/hydrogel composite layer in the hydrogel substrates.

The Friction Characterization: The friction test was performed on conventional ball-on-disk tribometer by recording the friction coefficient under different conditions at 25 °C by using TRB Tribometer (CSM, Switzerland). A stainless steel ball with a diameter of 6 mm was used as contact pair. The distance of one sliding cycle was 10 mm with a reciprocating mode and the friction coefficients were calculated by dividing the friction force by the applied normal load by the assistance of the software provided with the tribometer. All the tests were conducted using water lubricant.

Supporting Information

Supporting Information is available from the Wiley Online Library or from the author.

Acknowledgments

M.Rong and H. Liu contributed equally to this work. We gratefully acknowledge support from the National Key Research and Development Program of China (2016YFC1100401), the National Natural Science Foundation of China (51705507, 51805514) and the support of the Young Elite Scientists Sponsor Ship Program by CAST (2017QNRC0181). D. Dini thanks the Engineering and Physical Sciences Research Council (EPSRC) for support via his Established Career Fellowship (EP/N025954/1). M. Scaraggi thanks MIUR for the PRIN 2017 project support under the grant 2017948FEN (FASTire). F. Zhou thanks to the project support of Bureau of International Cooperation, Chinese Academy of Sciences (121B62KYSB2017009) and CAS (QYZDY-SSW-JSC013).

Received: ((will be filled in by the editorial staff))
Revised: ((will be filled in by the editorial staff))
Published online: ((will be filled in by the editorial staff))

References

[1] a) J. Klein, *Science* **2009**, *323*, *47*; b) C. P. Neu, K. Komvopoulos, A. H. Reddi, *Tissue Eng., Part B* **2008**, *14*, 235; c) C. W. McCutchen, *Wear* **1962**, *5*, 1; d) C. A. Poole, M. H. Flint, B. W. Beaumont, *J. Anat.* **1984**, *138*, 113; e) C. W. McCutchen, *The Joints and SynoVial Fluid* **1978**, *10*, 437.

[2] a) Y. Osada, J. P. Gong, *Adv. Mater.* **1999**, *10*, 827; b) X. Du, J. Zhou, J. Shi, B. Xu, *Chem. Rev.* **2015**, *115*, 13165.

[3] J. L. Drury, D. J. Mooney, *Biomaterials* **2003**, *24*, 4337.

[4] a) P. H. Corkhill, A. S. Trevett, B. J. Tighe, *Proc. Inst. Mech. Eng., Part H* **1990**, *204*, 147; b) M. Oka, K. Ushio, P. Kumar, K. Ikeuchi, S. H. Hyon, T. Nakamura, H. Fujita, *Proc. Inst. Mech. Eng., Part H* **2000**, *214*, 59; c) M. E. Freeman, M. J. Furey, B. J. Love, J. M. Hampton, *Wear* **2000**, *241*, 129; d) J. A. Stammen, S. Williams, D. N. Ku, R. E.

Guldberg, *Biomaterials* **2001**, *22*, 799; e) K. Yasuda, N. Kitamura, J. P. Gong, K. Arakaki, H. J. Kwon, S. Onodera, Y. M. Chen, T. Kurokawa, F. Kanaya, Y. Ohmiya, Y. Osada, *Macromol. Biosci.* **2009**, *9*, 307; f) K. L. Spiller, S. A. Maher, A. M. Lowman, *Tissue Eng., Part B* **2011**, *17*, 281; g) W. Zhao, X. Jin, Y. Cong, Y. Liu, J. Fu, *J. Chem. Technol. Biotechnol.* **2012**, *88*, 327.

[5] a) J. P. Gong, T. Kurokawa, T. Narita, G. Kagata, Y. Osada, G. Nishimura, M. Kinjo, *J. Am. Chem. Soc.* **2001**, *123*, 5582; b) D. Kaneko, T. Tada, T. Kurokawa, J. P. Gong, Y. Osada, *Adv. Mater.* **2005**, *17*, 535; c) Y. Wu, X. Pei, X. Wang, Y. Liang, W. Liu, F. Zhou, *NPG Asia Mater.* **2014**, *6*, e136; d) P. Lin, R. Zhang, X. Wang, M. Cai, J. Yang, B. Yu, F. Zhou, *ACS Macro Lett.* **2016**, *5*, 1191; e) S. Ma, M. Scaraggi, D. Wang, X. Wang, Y. Liang, W. Liu, D. Dini, F. Zhou, *Adv. Funct. Mater.* **2015**, *25*, 7366; f) J. P. Gong, *Soft Matter* **2006**, *2*, 544; g) M. Du, Y. Maki, T. Tominaga, H. Furukawa, J. P. Gong, Y. Osada, Q. Zheng, *Macromolecules* **2007**, *40*, 4313.

[6] X. Liu, H. Nanao, T. Li, S. Mori, *Wear* **2004**, *257*, 665.

[7] a) C. Zhang, Z. Ying, Q. Luo, H. Du, Y. Wang, K. Zhang, S. Yan, X. Li, Z. Shen, W. Zhu, *J. Polym. Sci., Part A: Polym. Chem.* **2017**, *55*, 2027; b) H. Chen, F. Yang, Q. Chen, J. Zheng, *Adv. Mater.* **2017**, *29*, 1606900; c) T. L. Sun, T. Kurokawa, S. Kuroda, A. B. Ihsan, T. Akasaki, K. Sato, M. A. Haque, T. Nakajima, J. P. Gong, *Nat. Mater.* **2013**, *12*, 932; d) Q. Chen, L. Zhu, C. Zhao, Q. Wang, J. Zheng, *Adv. Mater.* **2013**, *25*, 4171; e) J. Y. Sun, X. Zhao, W. R. Illeperuma, O. Chaudhuri, K. H. Oh, D. J. Mooney, J. J. Vlassak, Z. Suo, *Nature* **2012**, *489*, 133; f) T. Huang, H. G. Xu, K. X. Jiao, L. P. Zhu, H. R. Brown, H. L. Wang, *Adv. Mater.* **2007**, *19*, 1622; g) A. Nakayama, A. Kakugo, J. P. Gong, Y. Osada, M. Takai, T. Erata, S. Kawano, *Adv. Funct. Mater.* **2004**, *14*, 1124; h) K. Y. Gong J P, Kurokawa T, *Adv. Mater.* **2003**, *15* 1155; i) T. T. Haraguchi K, *Adv. Mater.* **2002**, *14*, 1120.

[8] P. Lin, S. Ma, X. Wang, F. Zhou, *Adv. Mater.* **2015**, *27*, 2054.

[9] P. Lin, T. Zhang, X. Wang, B. Yu, F. Zhou, *Small* **2016**, *12*, 4386.

[10] a) M. Chen, W. H. Briscoe, S. P. Armes, J. Klein, *Science* **2009**, *323*, 1698; b) U. Raviv, S. Giasson, N. Kampf, J.-F. Gohy, R. Jérôme, J. Klein, *Nature* **2003**, *425*, 163.

[11] M. A. Kelly, D. C. Fithian, K. Y. Chern, V. C. Mow, presented at Biomechanics of Diarthrodial Joints, springer, NY, **1990**.

[12] R. Tadmor, J. Janik, J. Klein, L. J. Fetters, *Phys. Rev. Lett.* **2003**, *91*, 115503.

[13] a) S. Jiang, Z. Cao, *Adv. Mater.* **2009**, *22*, 920; b) J. C. Hower, M. T. Bernards, S. Chen, H.-K. Tsao, Y.-J. Sheng, S. Jiang, *J. Phys. Chem. B* **2009**, *113*, 197.

[14] T. Moro, Y. Takatori, K. Ishihara, T. Konno, Y. Takigawa, T. Matsushita, U.-i. Chung, K. Nakamura, H. Kawaguchi, *Nat. Mater.* **2004**, *3*, 829.

[15] T. Du, B. Li, X. Wang, B. Yu, X. Pei, T. S. Huck Wilhelm, F. Zhou, *Angew. Chem., Int. Ed.* **2016**, *55*, 4260.

[16] a) V. C. Mow, S. C. Kuei, W. M. Lai, C. G. Armstrong, *J. Biomech. Eng.* **1980**, *102*, 73; b) M. R. DiSilvestro, Q. L. Zhu, M. Wong, J. S. Jurvelin, J.-K. F. Suh, *J. Biomech. Eng.* **2001**, *123*, 191; c) L Mattei, E. Campioni, M. A. Accardi, D. Dini, *Comput. Method. Biomech.* **2014**, *17*, 1553.

[17] Z. Sun, E. Feeney, Y. Guan, S. G. Cook, D. Gourdon, L. J. Bonassar, D. Putnam, *Proc. Natl. Acad. Sci. U. S. A.* **2019**, *116*, 12437.

The table of contents entry: Cartilage mimicking bi-layer material is engineered, which is capable of attaining low friction coefficient (order 0.010) under heavily loaded conditions (order 10 MPa contact pressure) and even can maintain low friction when subjected to 50k reciprocating cycles under high contact pressure with almost no surface wear in water environment, a performance incredibly close to that of natural articular cartilage.

Keyword: hydrogels, polymer brushes, sub-surface polymerization, low friction, high load-bearing

Author: *Mingming Rong, Hui Liu, Michele Scaraggi, Yanyan Bai, Luyao Bao, Shuanhong Ma*, Zhengfeng Ma, Meirong Cai, Daniele Dini, Feng Zhou**

High lubricity meets load capacity: Cartilage mimicking bilayer structure by brushing up stiff hydrogels from sub-surface

TOC Figure

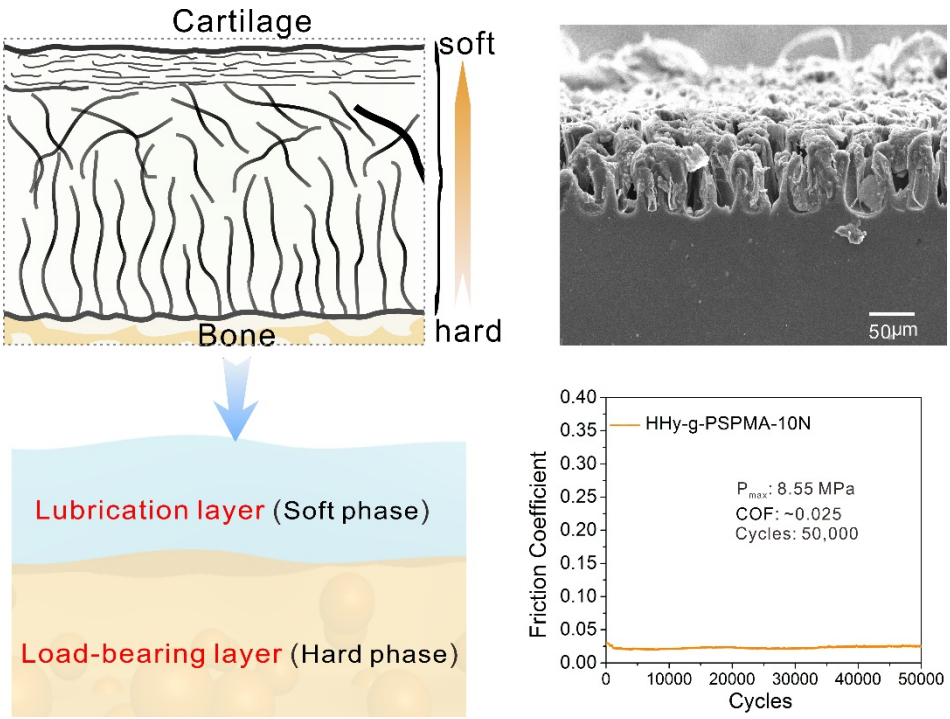

((Supporting Information can be included here using this template))

Supporting Information

High lubricity meets load capacity: Cartilage mimicking bilayer structure by brushing up stiff hydrogels from sub-surface

Mingming Rong[#], Hui Liu[#], Michele Scaraggi, Yanyan Bai, Luyao Bao, Shuanhong Ma, Zhengfeng Ma, Meirong Cai[1], Daniele Dini*, Feng Zhou**

Dr. M. Rong, Dr. H. Liu, Dr. Y. Bai, Dr. L. Bao, Dr. Z. Ma, Prof. S. Ma, Prof. M. Cai, Prof. F. Zhou
State Key Laboratory of Solid Lubrication, Lanzhou Institute of Chemical Physics, Chinese Academy of Sciences, Lanzhou, 730000, China
E-mail: zhouf@licp.cas.cn; mashuanhong@licp.cas.cn

Dr. M. Rong, Dr. H. Liu, Dr. Y. Bai
China University of the Chinese Academy of Sciences, Beijing, 100049, China

Dr. Y. Bai, Prof. M. Scaraggi
Università del Salento, 73100 Monteroni-Lecce, Italy, EU

Prof. M. Scaraggi
Istituto Italiano di Tecnologia (IIT), Center for Bio-Molecular Nanotechnologies, 73010 Arnesano (Lecce), Italy, EU

Prof. D. Dini, Prof. M. Scaraggi
Imperial College of London, London SW7 2AZ, United Kingdom
E-mail: d.dini@imperial.ac.uk

Supplementary Information Text

S1. Experimental results

Figure S1 shows the FT-IR spectra of different samples, including HHy, Hy-Br, HHy-Br, HHy-g-PSPMA and HHy-g-PSBMA. The asymmetrical stretching vibration signals at 1737 cm^{-1} on both FT-IR spectra of Hy-Br and HHy-Br samples are ascribed to the C=O bond of ester groups, which indicate the successful implant of BrMA in the bulk hydrogels polymer network. However, their strength on HHy-Br are obviously weaker than those in Hy-Br spectrums. This signal attenuation can be attributed to the strong shrinkage of polymer network induced by the ionic coordination between Fe^{3+} and COO^-.

Figure S2 shows the XPS spectra of samples. By compared with the pure hydrogel (Hyy), the appearance of Br3d peak at 70 eV indicates that the successful attachment of the ATRP initiator in the network of Hy-Br and HHy-Br. In addition, the existence of K2p peak at 293 eV and S2p peak at 168 eV clearly demonstrate the successful grafting of PSPMA polymer brushes on surface of HHy-Br.

Figure S3 shows the fine XPS spectra of N1s for the different samples. The N1s peak shows obvious shift (400.2 eV) after grafting PSBMA brushes compared with other four spectrums (399.6 eV), which is attributed to the appearance of charged N^+ element on PSBMA side chains.

Figure S4 shows the friction coefficient curve on the surface of bare HHy-Br hydrogels sample without grafting polymer brushes at applied load of 10 N.

Figure S5 shows the friction coefficients of HHy-g-PSPMA and HHy-g-PSBMA with different BrMA concentration. The polymerization time of the samples is 40 min. The friction tests were carried out with steel ball (6 mm diameter) at applied load 5 N and reciprocating frequency 1 Hz. From the figures below, it can be seen that the friction coefficients of HHy-g-PSPMA and HHy-g-PSBMA samples can separately achieve to 0.011 and 0.013 when the BrMA concentration was 0.5 wt%. Meanwhile, friction coefficients for both of them varied slightly between 0.010~0.013 with increasing the BrMA concentration, which is much smaller than the samples without BrMA. Such excellent lubricious performance of the two samples are owing to the high hydration of charged PSPMA and PSPMA brushes chains in HHy-g-PBs composite layer, originating from extraordinary water-lubrication mechanism.

Figure S6 shows the friction curves of HHy-g-PSPMA sample under the different loads during the 10k cycles. The friction coefficients of HHy-g-PSPMA sample are almost stable at ~0.014 and 0.016 under the normal loads of 5 N and 10 N, respectively. However, it is observed the

initial friction coefficient increased to ~0.028 at applied load of 20 N with the local maximum hertz contact stress of 10.75 MPa. Under such a condition, the friction coefficient of the sample increased gradually with the sliding cycles but no exceeded 0.060.

Figure S7shows the friction curves of HHy-g-PSBMA sample under the different loads during the 10k cycles. The friction coefficient of HHy-g-PSBMA sample is separately ~0.020 and ~0.024 under 5 N and 10 N, while the initial coefficient value reach ~0.030 but lower than 0.050 ultimately at applied load of 20 N.

Figure S8 shows the friction coefficient of HHy-g-PSBMA sample under the load of 10 N at 50k cycles. At first 18k cycles, the friction coefficient of HHy-g-PSBMA sample maintained at a lower level, which nevertheless kept increasing to close to 0.050 between 18k and 40k cycles, and then keep steadily after 50k cycles.

Figure S9 shows the surface wear morphology of the bare stiff hydrogels without brush grafting. Corresponding optical image (scale bar: 200 μm) and photography to show the wear morphology after getting through 3500 sliding cycles at applied load of 10 N.

S2. Numerical modelling

The rough contact mechanics is solved by employing the Persson's multiscale (statistic) contact mechanics[1] for layered materials[2]. The interaction at the macroscopic scale is instead solved with a Residual Molecular Dynamics (RMD) numerical model developed elsewhere[1b] by some of us and here extended and applied to our composite viscoelastic hydrogel sliding contact. In the following, we report a summary of the model.

In Figure S10 we show the schematic of the contact geometry in the macroscale contact model. The latter is characterized by the interaction between a rigid ideally smooth indenter in steady sliding contact with a compliant layered viscoelastic substrate. The local interface separation $u(\mathbf{x})$, corresponding to the local distance between the mating surfaces, is:

$$u(\mathbf{x}) = w(\mathbf{x}) - h(\mathbf{x}) - \delta, \tag{1}$$

where δ is the indenter penetration, $w(\mathbf{x})$ the surface elastic normal displacement, $h(\mathbf{x})$ the ball surface. The relation between separation $u(\mathbf{x})$ and contact pressure $\sigma_c(\mathbf{x})$ is computed within the Derjaguin's approximation [1b], and it can be written in term of a generic interaction law [2a]

$$\sigma(u) = f(u) \tag{2}$$

In this work we have adopted the (integrated) repulsive term of the L-J potential in Eq. 2 to simulate the adhesionless interaction, however adhesive interactions can be simulated as well. The surface elastic normal displacement $w(\mathbf{x})$ can be easily linked to the contact pressure in the Fourier space. In particular, upon defining the following Fourier transform (q is the transformed variable of x)

$$w(\mathbf{q}) = (2\pi)^{-2} \int d^2\mathbf{x}\ w(\mathbf{x}) e^{-i\mathbf{q}\cdot\mathbf{x}}$$

and

$$\sigma(\mathbf{q}) = (2\pi)^{-2} \int d^2\mathbf{x}\ \sigma(\mathbf{x}) e^{-i\mathbf{q}\cdot\mathbf{x}},$$

where $\sigma(\mathbf{x})$ is the interface pressure distribution (observed in the fixed reference), we have the following simple equation in the Fourier space

$$w(\mathbf{q}) = M_{zz}(\mathbf{q})\sigma(\mathbf{q}), \tag{3}$$

where $M_{zz}(\mathbf{q})$ is the surface response of the compliant substrate. $M_{zz}(\mathbf{q})$ depends on the rheological and geometrical properties of the substrate, as reported in the following for completeness.

Eqs. 1 to 3 are discretized on a regular square mesh of grid size δ in term of a residuals molecular dynamics process (RMD), and solved with a velocity Verlet integration scheme.

For our system, i.e. a coated viscolelastic half space, $M_{zz}(\mathbf{q})$ has the following analytical solution

$$\frac{M_{zz}(\mathbf{q},\omega)}{2/[E_r(\omega)q]} = n\frac{c_1 n_0 + c_2\left(n_1 M p^2 + 2n_2 mp + n_3 \varepsilon_p m^2\right)}{c_1 d_0 + c_2\left(d_1 M p^2 + 2d_2 mp + d_3 \varepsilon_p m^2\right)}, \tag{4}$$

where $\omega = \boldsymbol{q}\cdot\boldsymbol{v}_0$ ($\boldsymbol{v}_0$ relative contact sliding speed) and c_1, c_2, d_1, d_2, n_1, n_2, ε_p, m, n, p, and M are defined in Ref [2b], Appendix A2. $E_r(\omega)$ is the reduced complex viscoelastic modulus of the coating.

The macroscale contact model above allows to calculate the apparent contact area as well as the apparent contact pressure between the indenter and the composite gel. The true contact area is determined by using the Persson's multiscale rough contact mechanics. In particular, the true contact area is given by

$$\frac{A_c}{A_0} = \mathrm{erf}\left(\frac{1}{2\sqrt{G}}\right), \tag{5}$$

where

$$G(q_1) = \frac{1}{2\sigma_0^2}\int_{q_0}^{q_1} d^2q\, \frac{C(\mathbf{q})}{|M_{zz}(\mathbf{q}, \mathbf{q}\cdot\mathbf{v}_0)|^2}, \tag{6}$$

and where the roughness power spectral density $C(\mathbf{q})$

$$C(\mathbf{q}) = \frac{(2\pi)^2}{A_0}\langle h(\mathbf{q})h(-\mathbf{q})\rangle.$$

In Eq. 6 σ_0^2 is the macroscopic contact pressure distribution calculated with the above mentioned macroscale contact model.

In the main text, an isotropic roughness is assumed to cover the composite gel, with self-affine high-frequency range in addition to a roll-off region in the frequency range [q_0, q_r], mimicking the real system. Moreover, the root mean square roughness h_{rms} is varied in the range 1, 10 or 100 μm, with low frequency cutoff q_0= 0.625E+03 m^{-1}, roll-off q_r= 0.100E+07 m^{-1} and high frequency cut off q_1= 0.320E+08 m^{-1}. The fractal dimension D_f=2.2 in the range of q_r to q_1. The spherical indenter is assumed to be rigid and smooth (compared to the composite lubrication layer), with a 6 mm diameter. The substrate hydrogel layer is modelled as a bulk material with elastic modulus of 40 MPa. In order to consider the dissipation dynamics related to the weeping mechanism, the hydrated layer (on the top of the stiffer bulk) is assumed viscoelastic with an elastic modulus in the rubbery regime of $E_0 \approx 10$ kPa [3] and (one) relaxation time $\tau_r \approx 1$ ms. The elastic modulus in the glassy regime is strongly dependent on the actual porosity φ of the system, and can be approximately described by $E_\infty \approx E_0(1-\varphi)^{-1}$. We have assumed a representative porosity value $\varphi = 1/2$, leading to a glassy regime elastic modulus of 20 kPa.

In Figure S11 we show, for the macroscopic interaction, the apparent (i.e. nominal) contact area as a function of the squeezing load for different values of the composite top layer thickness (1, 10 and 100 μm) and for three sliding speeds (1, 10 and 100 mm/s), whereas the other contact parameters are similar to those adopted in the main text.

Increasing the sliding speed determines a stiffening of the composite top layer, leading to a reduction of the contact area, with larger decrease for the thicker coating.

In Figure S12 we report the apparent solid contact pressure field p_0, the mean contact pressure (red curve) and the corresponding squeezing load F_N, for the system studied in Figure 5(B.2).

S3. Calculation for maximum Herzt contact pressure (P_{max})

The p_{max} is the maximum Herzt contact pressure which is applied at the apex of indentator, which can be calcualted by Eq. 7

$$p_{max} = \frac{3F}{2\pi a^2} = \frac{1}{\pi}\left(\frac{6FE^{*2}}{R^2}\right)^{\frac{1}{3}} \quad (7)$$

Where F is the applied load and *R* is the radius of steel ball (*R*=3 mm). $E^*$is the integrated elastic modulus based on two kinds of materials, which can calculated by

$$\frac{1}{E^*} = \frac{1-{v_1}^2}{E_1} + \frac{1-{v_2}^2}{E_2} \quad (8)$$

Where E_1, E_2 is separately the elastic modulus of stiff HHy-Br hydrogel and steel ball (314#), v_1, v_2 is separately their Poisson's ratios. For steel ball in current work, E_2 is ~195 GPa, v_2 is 0.247, the rigid sphere can be viewed as no deformation when contacting with the elastic hydrogel substrate. v_1 is ~0.5, E_1 is ~40 Mpa by calculating the linear slope at tensile and compressive tests curves. Because the calcuated result of $\frac{1-{v_2}^2}{E_2}$ is approximately to 0, also due to $E_2 \gg E_1$, this term has little influence on the calculation result of E^*. Then we can obtain the value of E^*, it is 53.92 MPa.

Finally, the P_{max} under different loads were obtained by Eq. 7, as shown in Table S1.

Figure S1-Figure S12

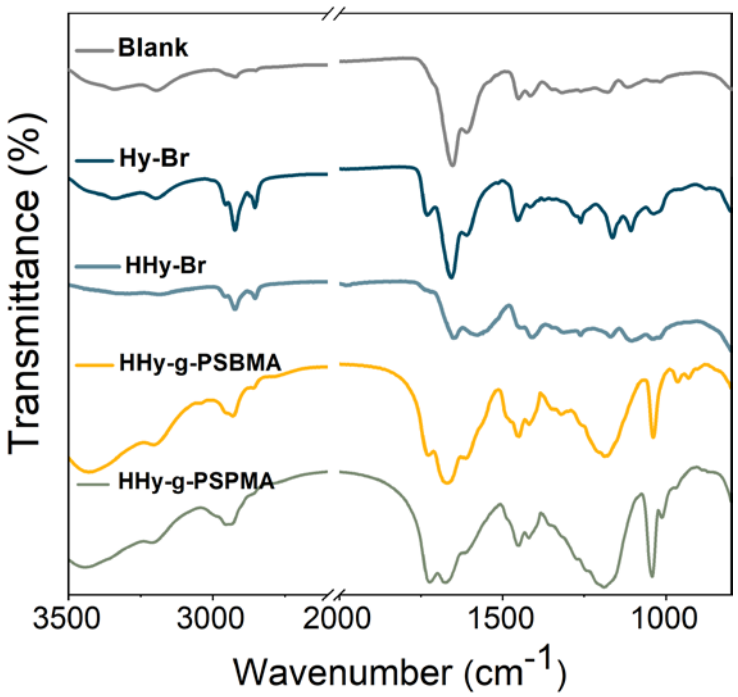

Figure S1. FT-IR spectra of different samples: Blank (HHy), Hy-Br, HHy-Br, HHy-g-PSBMA and HHy-g-PSPMA.

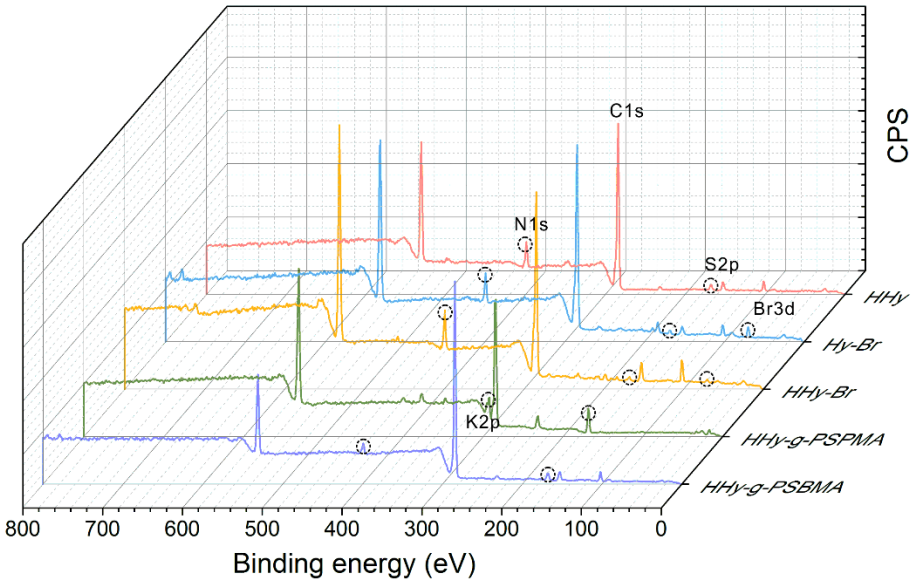

Figure S2. The XPS spectra of different kinds of samples including HHy, Hy-Br, HHy-Br, HHy-g-PSPMA and HHy-g-PSBMA.

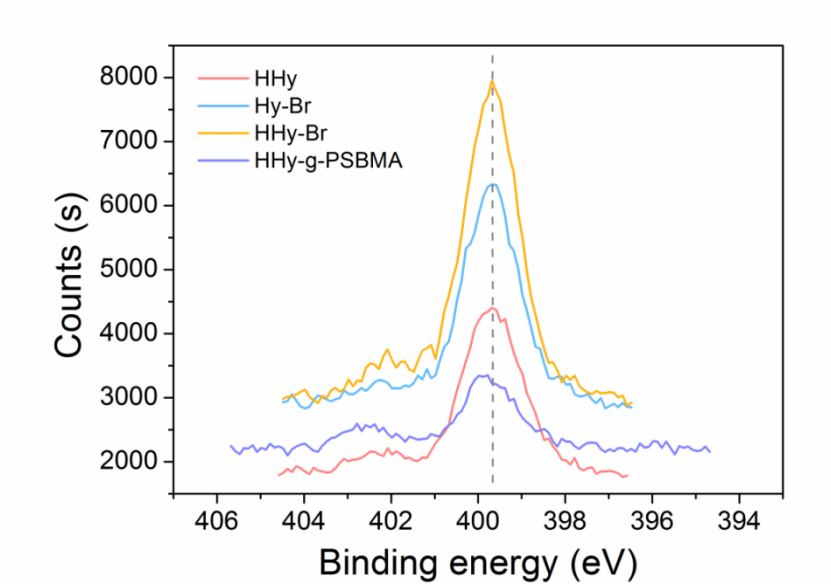

Figure S3. Fine XPS spectra of $N1_S$ for different samples: HHy, Hy-Br, HHy-Br, HHy-g-PSBMA. The slightly shift at 400 eV on HHy-g-PSBMA compared with other four spectra illustrates the existence of N^+ which further confirms the hydrogel substrate successfully modified with PSBMA brushes.

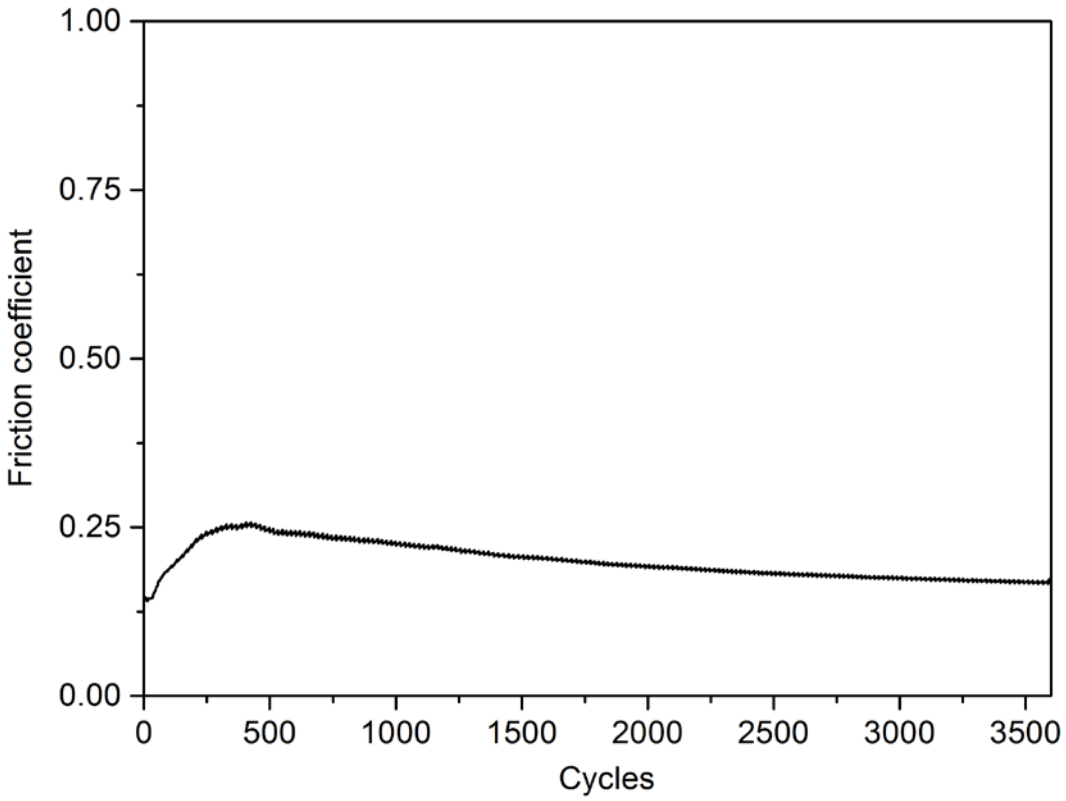

Figure S4. The friction coefficient curve on the surfaces of HHy-Br hydrogels sample without grafting polymer brushes at applied load of 10 N.

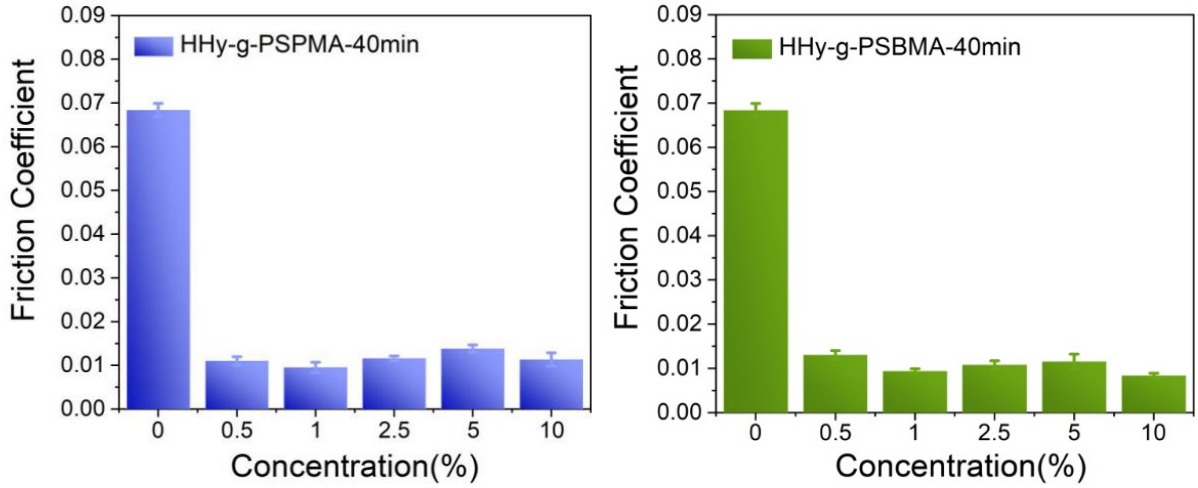

Figure S5. The friction coefficients of the layered HHy-g-PSPMA and HHy-g-PSBMA samples with different BrMA concentration. The polymerization time of samples is 40 min. Friction tests above were carried out with steel ball (Φ 6 mm) at applied load 5 N and reciprocating frequency 1 Hz.

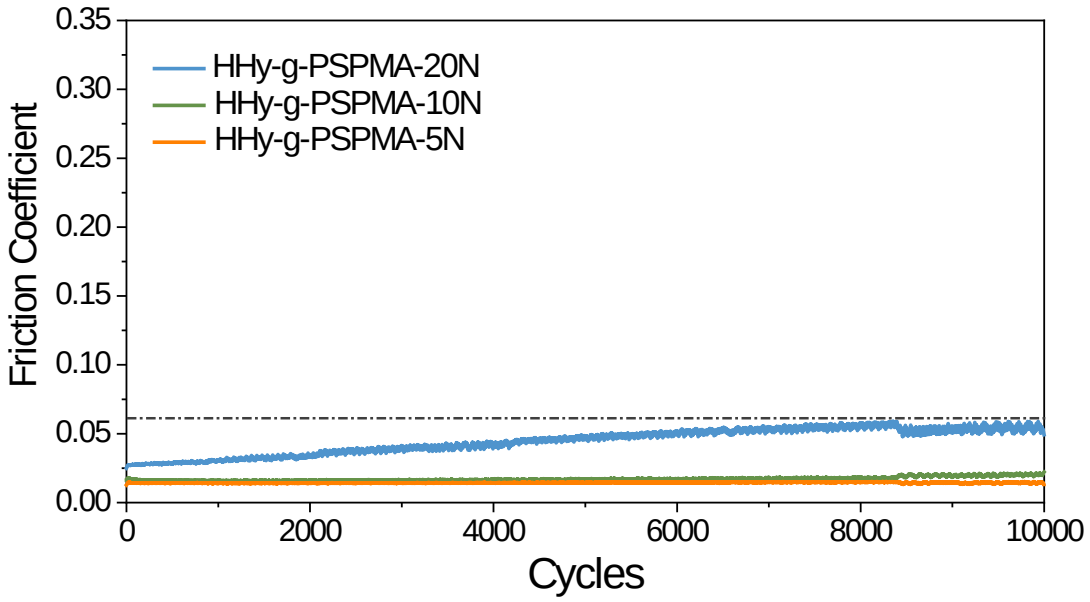

Figure S6. Friction curves of HHy-g-PSPMA sample under the normal load of 5 N (P_{max}: 6.78 MPa), 10 N (P_{max}: 8.55 MPa) and 20 N (P_{max}: 10.77 MPa) during the 10,000 sliding cycles.

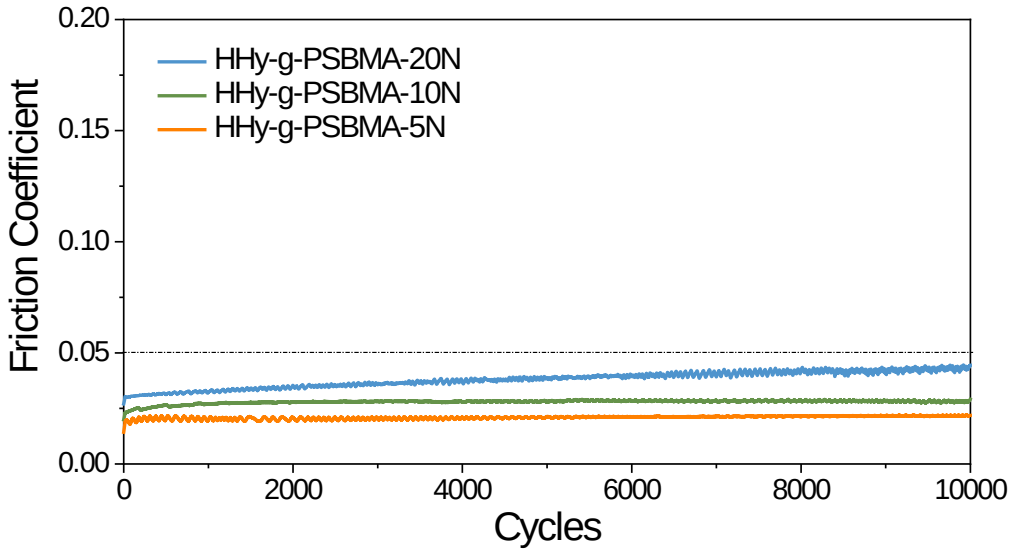

Figure S7. Friction curves of HHy-g-PSBMA sample under the normal load of 5 N (P_{max}: 6.78 MPa), 10 N (P_{max}: 8.55 MPa) and 20 N (P_{max}: 10.77 MPa) during the 10,000 sliding cycles.

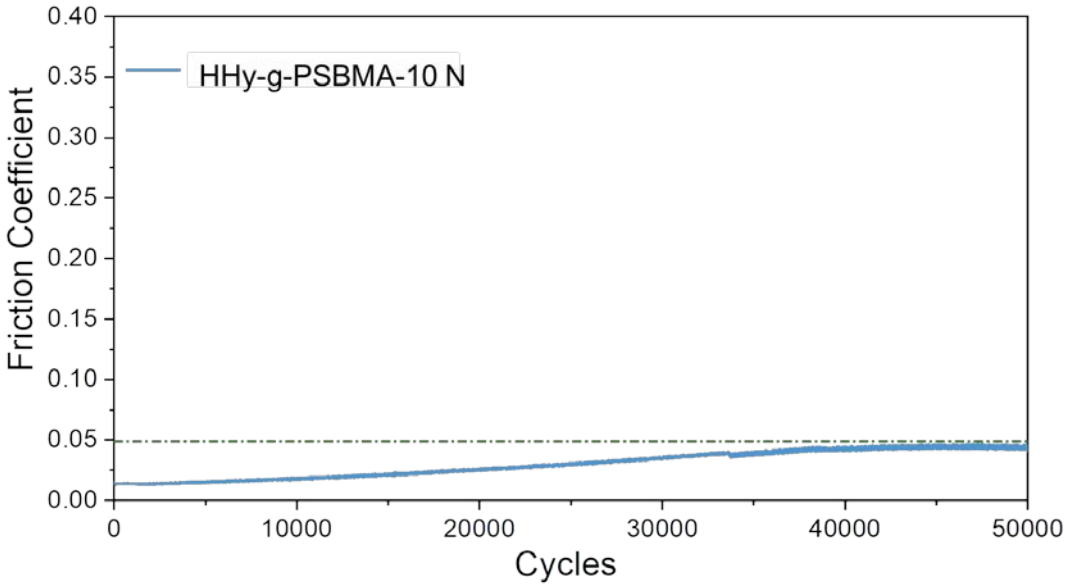

Figure S8. The friction coefficient-cycles curve on the surfaces of HHy-g-PSBMA for 50,000 friction cycles at applied load 10 N.

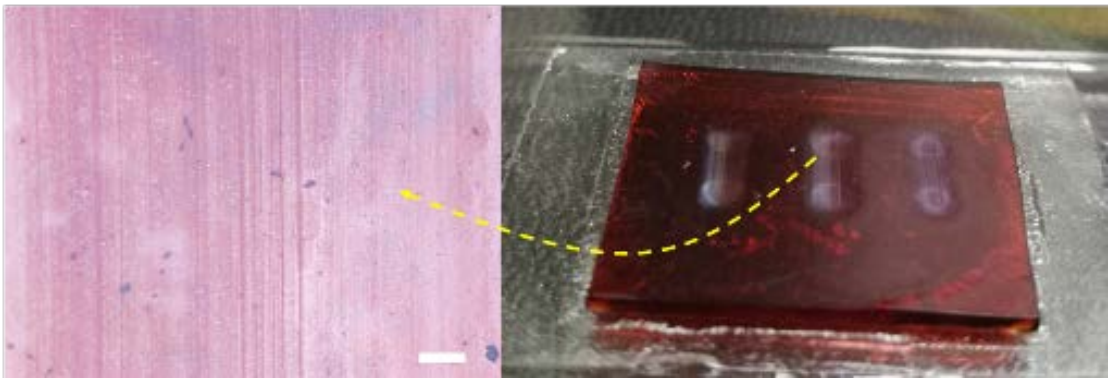

Figure S9. Corresponding optical image (scale bar: 200 μm) and photography show the wear morphology of the bare stiff hydrogels without brush grafting after getting through 3500 sliding cycles at applied load of 10 N.

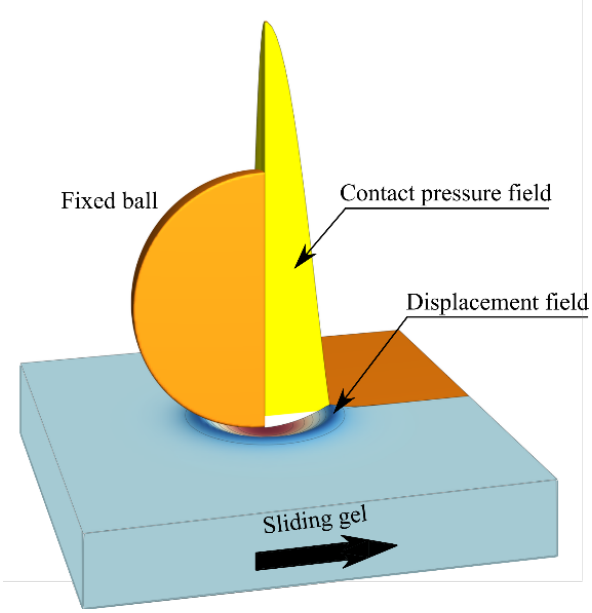

Figure S10. Contact setup for the macroscale contact model. The composite gel substrate is in relative sliding contact with a smooth rigid indenter, squeezed in contact at constant load F_N.

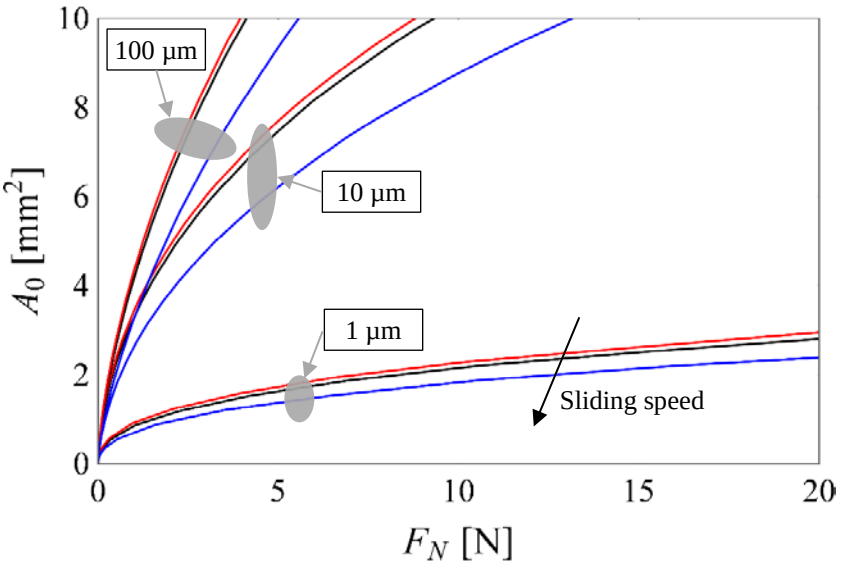

Figure S11. Nominal contact area as a function of squeezing load, for three coating thickness (1, 10 and 100 µm) and three sliding speeds (1, 10 and 100 mm/s).

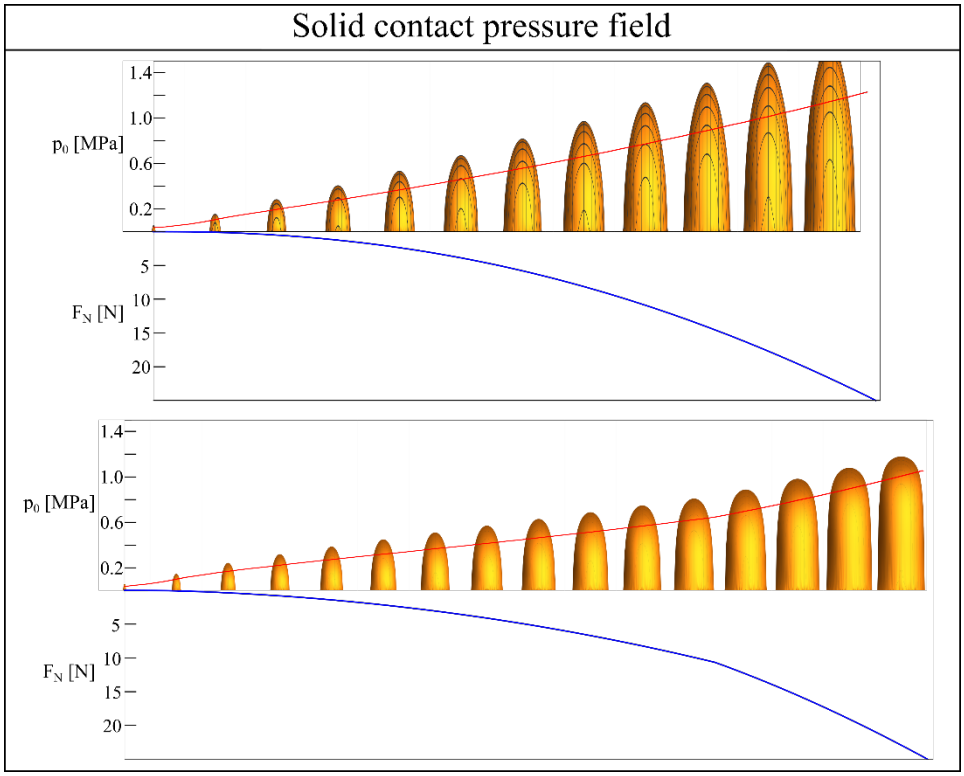

Figure S12. Apparent solid contact pressure field p_0, the mean contact pressure (red curve) and the corresponding squeezing load F_N, for the system studied in Figure 5(B.2). Top: HHy-g-PSPMA. Bottom: HHy-g-PSBMA.

LOAD (N)	1	3	5	7	10	20
P_{max} (MPa)	3.97	5.72	6.78	7.59	8.55	10.77

Table S1. Calculation of the maximum Hertz contact stresses (P_{max}) at the interface of the steel ball against the sample at different normal loads.

System	Contact load/pressure	Wear	Friction	Lubricant	Notes	Experimental setup	Ref.
Natural articular cartilage	1 to 20 MPa	N	0.001 to 0.03	synovial fluid	high load-bearing capacity, low friction, wear-resistance	-	[4]
Polymer brushes (note: limited capacity of polymer brushes to support high loads at macroscale with rough surfaces)	10 mN, 7.5 MPa	H	~ 0.0004	water	low friction, high load-bearing capacity	smooth mica vs smooth mica; SFA model system	[5]
	0.49 N	H*	~ 0.02	water	low friction	ball on disk, with glass ball vs Si; Macro-tribometer	[6]
	-	H	~ 0.1	bovine calf serum	wear-resistance	CoCrMo head vs PE; hip-joint simulator	[7]
Hydrogels (note: Coexistence of low friction, high load-bearing capacity and wear-resistance are unlikely for hydrogels)	6 to 20 N	H	0.05 to 1.7	water	high load-bearing capacity	ball on disk, with steel ball vs gel; macro-tribometer	[8]
	less than 0.1 MPa	N	0.001 to 0.01	water	low friction	disk on disk, with gel vs gel; rheometer	[9]
	~ 0.1 MPa	N	0.0001 to 0.001	water	low friction	disk on disk, with gel vs gel; rheometer	[10]
	0.1 to 1 N, less than 1 MPa	H	~ 0.28	water	wear-resistance	disk on disk, with gel vs gel; rheometer	[11]
	40 N, ~ 2 MPa	H**	0.006	water	high load-bearing capacity, low friction	ball on disk, with PDMS ball vs gel; macro-tribometer	[12]
Entangled polymer	1 to 20 N, 3 to 10 MPa	N	0.008 to 0.03	water	**high load-bearing**	ball on disk, with steel	**this work**

brushes and hydrogel composite					**capacity, low friction, wear-resistance**	ball vs composite gel; macro-tribometer	

Table S2. Articular cartilage mimicking prototypes reported in literature. *N*, *H* symbols in *Wear* column refer to *no* and *high*, respectively. *Heavy damage after 450 contact cycles. **Heavy damage after 10k cycles.

References

[1] a) B. N. J. Persson, *J. Chem. Phys.* **2001**, *115*, 3840; b) B. N. J. Persson, M. Scaraggi, *J. Chem. Phys.* **2014**, *141*, 124701; c) M. Scaraggi, B. N. J. Persson, *J. Chem. Phys.* **2015**, *143*, 224111.

[2] a) B. N. J. Persson, *J. Phys.: Condens. Matter* **2012**, *24*, 095008; b) M. Scaraggi, D. Comingio, *Int. J. Solids Struct.* **2017**, *125*, 276.

[3] B. N. J. Persson, *Eur. Phys. J. E* **2010**, *33*, 327.

[4] S. Jahn, J. Seror, J. Klein, Annu. *Rev. Biomed. Eng.* **2016**,*18*, 235.

[5] M. Chen, W.H. Briscoe, S.P. Armes, J. Klein, *Science* **2009**, *323*, 1698.

[6] M. Kobayashi, M. Terada, A. Takahara, *Faraday Discuss*. **2012**, *156*, 403.

[7] T. Moro, Y. Takatori, K. Ishihara, T. Konno, Y. Takigawa, T. Matsushita, U. I. Chung, K. Nakamura, H. Kawaguchi, *Nat. Mater.* **2004**, *3*, 829.

[8] M. E. Freeman, M. J. Furey, B. J. Love, J. M. Hampton, *Wear* **2000**, *241*, 129.

[9] J. P. Gong, T. Kurokawa, T. Narita, G. Kagata, Y. Osada, G. Nishimura, M. Kinjo, *J. Am. Chem. Soc.* **2001**, *123*, 5582.

[10] D. Kaneko, T. Tada, T. Kurokawa, J.P. Gong, Y. Osada, *Adv. Mater.* **2005,** *17*, 535.

[11] I. C. Liao, F. T. Moutos, B. T. Estes, X. Zhao, F. Guilak, *Adv. Funct. Mater.* **2013**, *23*, 5833.

[12] S. Ma, M. Scaraggi, D. Wang, X. Wang, Y. Liang, W. Liu, D. Dini, F. Zhou, *Adv. Funct. Mater.* **2015**, *25*, 7366.